Karlsruhe Institute of Technology

Institute of Fluid Mechanics
Institute of Fluid Mechanics
Geb. 10.23, 6.OG, Kaiserstraße 10, 76131 Karlsruhe
http://www.istm.kit.edu

CFD Simulation of an Air Bubble in Microfluidics using Volume of Fluid and Phase Field Methods in OpenFOAM

Numerische Simulation einer Luftblase in der Mikrofluidik mit der Volume of Fluid und Phasenfeld-Methode in OpenFOAM

Master Thesis of

Farshid Jamshidi

At the Department of Mechanical Engineering,
Institute of Fluid Mechanics

Advisors: M.Sc. Hans Heimel
Dr.-Ing. Manuel Hasert
Dr.-Ing. Martin Wörner
Prof. Dr.-Ing. Bettina Frohnapfel

Duration: March 2016 – July 2016

I declare that I have developed and written the enclosed thesis completely by myself, and have not used sources or means without declaration in the text.

Karlsruhe, 15. 07. 2016

.....

(**Farshid Jamshidi**)

Preface

I am a student of mechanical engineering at Karlsruhe Institute of Technology (KIT), Karlsruhe, Germany and this is my master's thesis on numerical simulations of an air bubble in microfluidic channels in the Institute of Fluid Mechanics (in German: Institut für Strömungsmechanik(ISTM)) under the supervision of Prof. Bettina Frohnapfel, the head of ISTM, whom I thank very much for her time and help.

The project was in industry, i.e., funded by Festo AG. & Co. KG in Esslingen, Germany. It was in Computer Aided Engineering (CAE) of the company and a part of Mr. Hans Heimel's PhD program. I would like to thank him for his availability and assistance. I also thank Dr. Manuel Hasert for his help and consistent guidance during this project. I am thankful to Mr. Andreas Schleth, CAE head, for his support and letting me to have flexible working hours.

Dr. Martin Wörner is the head of Multiphase Flow Group in Institute of Catalysis Research and Technology at KIT. He is an amazing supervisor and I really appreciate his nice way of supervision of this thesis. Xuan Cai, one of his PhD students, helped me in many occasions. Therefore, I would like to thank him and also Dr. Holger Marschall, the head of Junior Research Group "Advanced Two-Phase and Interfacial Flow Simulations using OpenFOAM" at Technical University of Darmstadt, who guided me so many times.

"If I have seen further, it is by standing on the shoulders of giants."

– Isaac Newton

Farshid Jamshidi
July 15, 2016

Abstract

The major problem regarding numerical simulation of multiphase flows in microfluidic systems are discrepancies in the results with the ones obtained by the same numerical approaches in larger scales. Several potential causes such as the effect of confining boundaries, large curvature of interfaces or small sizes of dispersed phases are reported elsewhere. To determine the effect of these properties on numerical results, a sensitivity analysis on the most important parameters affecting the fluid dynamics of a microfluidic multiphase system is required.

The aim of this thesis is to compare the Volume of Fluid (VOF) and Phase Field methods implemented in OpenFOAM package, in solvers $interFoam$ and $phaseFieldFoam$, respectively, in terms of their basic suitability to simulate multiphase flows. For this purpose, $interFoam$ in foam-extend-3.1 and $phaseFieldFoam$ in OpenFOAM-1.6-ext are used. By doing so, problematic parameters of microfluidic multiphase simulations can be identified. The case study of interest is a two dimensional motionless air bubble in stagnant water. This configuration is frequently discussed in literature as a validation case. The simplicity of this case makes it suitable as a fast benchmark to achieve the target of this study. The starting point of the research is therefore the comparison between the numerical results obtained for this configuration with the ones reported in literature. For this benchmark problem, mismatch between discretised surface tension force and pressure gradient and/or inaccurate computation of interface curvature can lead to numerical errors, which manifest as parasitic currents. These currents strengthen when there exist discontinuities in field variables (e.g., density and pressure) at the interface between the air bubble and water. Thus, in the second step, this error and its consequences such as motion of bubble and distortion of its interface are characterised. To do so, several parameters such as spatial and temporal resolutions of the numerical solvers, initial estimation for bubble interface thickness and bubble diameter have been changed. The accuracy of the solvers is determined based on their ability to predict the pressure difference between the gas inside the bubble and the surrounding liquid and minimising the induced parasitic current and bubble motion, while maintaining an appropriate bubble interface thickness.

The results show that the $phaseFieldFoam$ is more accurate in predicting most of the characteristic properties of the considered multiphase system, compared to $interFoam$. Under mesh refinement, the former code converges with equal densities and viscosities but not for air-water system where the magnitude of spurious currents is independent from grid size. Furthermore, it is revealed that $phaseFieldFoam$ requires at least six computational cells across the thickness of bubble interface to provide accurate results. It is also shown that to achieve convergence, satisfying common criteria on the group of involved non-dimensional numbers (here, Courant and Cahn numbers) is not sufficient. A further restriction originates from the computational time step. By refining the time step, the diffusion number, which is shown to influence the solution significantly, can be controlled and as a result, convergence of the results can be obtained.

Moreover, the main drawback of $phaseFieldFoam$ is illustrated to be in conserving the mass of the gas phase inside the bubble as the solver tends to shrink the bubble size. This

problem, however, could be overcome by a higher mesh resolution. On the other hand, although *interFoam* does not suffer from problems in mass conservation, it is out of step in prediction of the characteristic parameters as well as in eliminating the parasitic current and unfavourable bubble motion. The adopted approach for tackling this problem is beneficial for numerical simulation of three-dimensional microfluidic systems with complex flow geometries, both for design and optimisation purposes.

Contents

1. Introduction

1.1. Motivation of the Work

In fluid mechanics, if the dimensions of a channel are tens to hundreds of micrometers, then it is labelled **microfluidics**. The smaller size, the less usage of expensive fluids for experiments in a wide variety of applications, such as molecular analysis, biodefense, molecular biology and microelectronics [1]. **Multiphase flows**, obvious from the name, are flows consisting of more than one phase, i.e., state like air bubbles or oil droplets in water. For different applications, e.g., measuring of ingredients of a mixture, it is desirable to understand the behaviour of phases and interactions between them. Fig. 1.1 illustrates schematically a device for measuring phosphate concentration. The fluid consists of phosphate and is on a microfluidic chip. The light originates from a light source and traverses the chip and goes to a spectrometer where its altered wave frequency can be measured. Based on the attenuation of the spectrum at a certain frequency, one can correlate the concentration of phosphate in the fluid on the chip. If there are air bubbles, they disturb the signal and diminish the accuracy of measurement. In worst cases, the larger air bubbles can clog the microfluidic channel. Therefore, a better understanding of bubble behaviour in microfluidics is necessary.

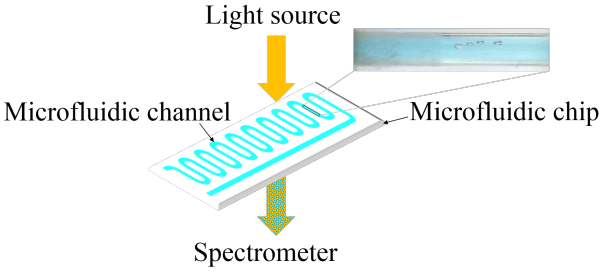

Figure 1.1.: Phosphate measurement.

To achieve this target, Computational Fluid Dynamics (CFD), specifically two different numerical methods, i.e., **Volume of Fluid** (VOF) and **Phase Field** methods are evaluated in this work. The mathematical framework of these two methods and their implementations in OpenFOAM which is an open source CFD software [2] will be explained in sections 2.2 and 2.3.

1.2. Some Concepts in Multiphase Flow Simulations

In the surface of a material, molecules have higher energy than in bulk because they are not bounded from all spatial sides. This excess energy of the surface molecules is called **surface energy** and tries to minimise the surface area. To phrase it differently, this is the energy to create new surfaces. In multiphase flows, the size of **interface** between two materials, where physical properties alter quickly, can be compared to the molecular separation scale. Deep in the liquid, the nearness of molecules results in repelling between them. But at the interface, because of fewer neighbours, there is an attraction between the other molecules and it is called **surface tension**, defined as the normal force per unit of length [3, 4], which is equal to surface energy density for a liquid. In this work, physical properties of phases and their changes over interface are investigated by means of OpenFOAM which uses finite volume method.

A **sharp interface** model means that the thickness of interface is zero like in Level-Set method and there is a jump, i.e., discontinuity of physical properties from one phase to another across the interface but in a **diffuse interface** model, a surface with a finite thickness is defined and physical quantities have smooth but rapid transition in a thin transition layer [5]. The motion and deformation of interface can be computed on fixed grids [6].

Numerical methods, here for describing the motion of interface, have numerical errors which cause non-physical velocities called **parasitic currents** expressed by Lafaurie et al. [7] for the first time. Some authors such as Francois et al. [8] named these flows spurious currents. In this work, some test cases, for example, an air bubble in equilibrium, Fig. 2.6, are simulated to quantify these errors. The origin of parasitic currents is imbalance between pressure gradient and surface tension force as well as an inaccurate estimation of interface curvature. In all test cases in this thesis, the initial velocity field is zero but at the end of simulation, there is a non-zero velocity field and the maximum value of velocity vectors, $|\mathbf{U}_{max}|$, is regarded as the maximum parasitic current.

1.3. Literature Review

Continuum Surface Force (CSF) model, introduced by Brackbill et al. [9], is one possible way for modelling surface tension effects on fluid motion. In this model

$$\mathbf{F}_\sigma = (\sigma \mathcal{K} \mathbf{n} + \nabla_s \sigma)\delta \tag{1.1}$$

where the l.h.s represents the surface tension force and in the r.h.s., σ is the surface tension coefficient, $\mathcal{K}$ the local mean curvature, $\mathbf{n}$ the unit vector normal to the interface, ∇_s the surface gradient and δ the delta function.

Lafaurie et al. [7] stated that a higher surface tension results in higher parasitic currents. Harvie et al. [10] explained the origin of the parasitic currents in detail and found that these currents cannot be always restricted by increasing space and time resolutions. Yokoi [11] proposed a numerical method to simulate free surface flows with complicated moving interfaces like droplet splashing. His framework is a density-scaled balanced CSF model to reach the lowest parasitic currents, which will be explained in section 3.1.2.

Deshpande et al. [12] investigated the performance of *interFoam* which is a solver for two-phase flow in OpenFOAM based on a modified VOF method. They found that this solver compute the curvatures which deviates about 10% from the analytical value. Albadawi et al. [13] also recognised that *interFoam* cannot deal appropriately with high surface tension effects. Thus, they coupled this solver with a Level-Set method to capture the interface and compute the surface tension more properly. In the Level-Set method, a

signed distance function categorised two phases from each other. This function is positive for one phase, negative for another and zero for the interface. Another extension of VOF method is the Moment of Fluid for the simulation of interface dynamics [14]. In addition to the interface reconstruction in VOF methods by tracking the cell-wise material volumes, the Moment of Fluid method tracks the cell-wise material centroids. This eventuate in obtaining more information about the interface reconstruction scheme where the volume is conserved.

Acar [15] explained that the Phase Field method is a method for describing the diffuse interface evolution which uses a 4^{th} order diffusion equation. In this model, the interface characteristics like thickness is controllable. Lee et al. [16] compared different types of delta functions for Phase Field models in several numerical experiments and found that the delta function $\delta(C) = |\nabla C|$ is the best in most cases where C is an order parameter for phase identification. Jacqmin [6], for using the Phase Field method, appended the surface tension force $-C\nabla\phi$ to the Navier-Stokes equations where ϕ the chemical potential of this variable. In his calculations, the interface is advected by a continuum advective-diffusion equation. Jacqmin [6] commented that Phase Field method is able and appropriate for two phase flow singularities, micro-scale modelling and even for simulation in nano-scale, which is the actual interface thickness. Moreover, He et al. [17] compared the CSF and chemical potential gradient models for formulation of surface tension force and found that the parasitic currents are lower by the latter model. As a drawback of Phase Field simulations, however, Yue et al. [18] expressed the spontaneous shrinkage of a drop or bubble while C of the bulk phases shifts from its values. This mass lost will be discussed in section 3.2.2.

2. Mathematical Framework and Numerical Methods

2.1. The Navier-Stokes Equations for Two-Phase Flow in Single Field Formulation

The continuity equation for two isothermal, immiscible, incompressible Newtonian fluids is defined as in [13]

$$\nabla \cdot \mathbf{U} = 0 \tag{2.1}$$

and the momentum equation

$$\frac{\partial(\rho \mathbf{U})}{\partial t} + \nabla \cdot (\rho \mathbf{U}\mathbf{U}) = -\nabla p + \nabla \cdot \tau + \mathbf{F}_b + \mathbf{F}_\sigma \tag{2.2}$$

where $\mathbf{U}$ is the fluid velocity vector, ρ the fluid density, t time, p the fluid pressure, τ the viscous stress tensor which is $\tau = \mu[(\nabla \mathbf{U}) + (\nabla \mathbf{U})^T]$ with μ as the fluid viscosity and $\mathbf{F}_b$ are body forces acting on the fluid such as gravity force. In this work, the gravity force is assumed to be zero but $\mathbf{F}_\sigma$ for multiphase flows is of interest. The phases are identified by a phase indicator function X and physical properties such as density and viscosity depend on this function. For this function there is a topological equation [19]

$$\frac{\partial X}{\partial t} + (\mathbf{U} \cdot \nabla) X = 0 \tag{2.3}$$

2.2. Volume of Fluid Method in OpenFOAM: interFoam

For free boundary configurations, e.g., interfaces between fluids, Hirt and Nicols [20] introduced VOF method in 1979. This numerical method for multiphase flows reconstruct the interface based on the values of an indicator function in the computational cells of a fixed mesh (an Eulerian mesh), i.e., a rectangular grid despite of interface shape [21]. This phase indicator function, i.e., a **volumetric phase fraction** function with the unit value for a cell fully occupied by liquid and zero value for a cell only by gas. Cells with volume phase fraction within these two distinct values are considered to specify the interface between two phases. From the cell values, the interface can be reconstructed. Fig. 2.1 shows the definition of an air bubble in water using VOF.

0.1	0.4	0.8	1
0	0	0.15	0.8
0	0	0	0.4
0	0	0	0.1

Figure 2.1.: Fluid representation in VOF based on volumetric phase fraction.

VOF method is implemented in OpenFOAM in a few solvers and one of them is called *interFoam* (IF) which is a solver for two incompressible, isothermal immiscible fluids [2]. The volumetric phase fraction in IF is $alpha1$ with $alpha1 = 1$ for liquid and $alpha1 = 0$ for gas. The physical properties, density ρ and viscosity μ can be written by using a weighted average of two phases

$$\rho = \rho_l \alpha + \rho_g (1 - \alpha) \tag{2.4}$$

$$\mu = \mu_l \alpha + \mu_g (1 - \alpha) \tag{2.5}$$

where $\alpha = alpah1$ is the volumetric phase fraction which is adevected algebraically in IF. It means that IF utilises a compressive scheme wherewith the r.h.s of Eq. (2.3) changes with an artificial anti-diffusion term as follows [13]

$$\frac{\partial \alpha}{\partial t} + (\mathbf{U} \cdot \nabla)\alpha = -\nabla \cdot (\alpha(1 - \alpha)\mathbf{U}_c) \tag{2.6}$$

where $\mathbf{U}_c = \mathbf{U}_l - \mathbf{U}_g$ is the vector of relative velocity, where $\mathbf{U}_l$ and $\mathbf{U}_g$ are liquid and gas velocities, respectively. The relative velocity is also determined as the compressive velocity. The r.h.s of Eq. (2.6) is important at the interface because of $\alpha(1 - \alpha)$ and is to mitigate the numerical smearing of physical properties over the interface. Fig. 2.2 illustrates changes of physical properties in normal direction to interface. It is obvious that with compression term, the solution is closer to the sharp interface.

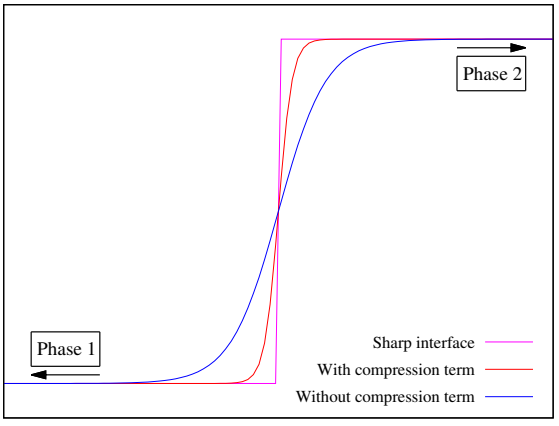

Figure 2.2.: Schematic illustration of discontinuity in physical properties across interface using VOF.

Furthermore, for higher compression a compressive factor, c_{alpha}, is defined like below [13]

$$\mathbf{U}_c = min(c_{alpha}|\mathbf{U}|, |\mathbf{U}_{max}|)\frac{\nabla \alpha}{|\nabla \alpha|} \tag{2.7}$$

In this work, $c_{alpha} = 1$ is always considered. For further information, a special method, namely MULES, in IF is applied in order to integrate the Eq. (2.6). MULES stands for multidimensional universal limiter for explicit solution.

Based on CSF model, for constant interfacial tension, σ, the surface tension force per unit interfacial is calculated by $\mathbf{f}_\sigma = \sigma\mathcal{K}(\alpha)\nabla\alpha$ where $\mathcal{K}(\alpha)$ is the mean surface curvature using updated α after Eq. (2.6) [13]. Hence, it is written $\mathcal{K}(\alpha) = -\nabla \cdot \mathbf{n}$ where $\mathbf{n}$ is defined by $\mathbf{n} = \nabla\alpha/|\nabla\alpha|$. This model is implemented in momentum equation (Eq. (2.2)) in IF and because of the spatial discretisation and curvature estimation, there exist parasitic currents in the vicinity of interface [21].

2.3. Phase Field Method in OpenFOAM: phaseFieldFoam

In Phase Field method, the phase identification for two incompressible, viscous and isothermal fluids is based on an order parameter, C, with $C_l = 1$ and $C_g = -1$ where l and g stand for liquid and gas, respectively [22]. Similar to VOF, cells with C within these values represent the cells belonging to the interface. Yue et al. [18] used Ginzburg-Landau functional for the the mixing energy of the two phase system on the computational domain Ω

$$\mathcal{F} = \int_\Omega \lambda \left[\frac{1}{2}|\nabla C|^2 + f(C)\right] d\Omega \tag{2.8}$$

where λ is the mixing energy density and $f(C)$ is a double well potential function. The first term in r.h.s of Eq. (2.8) is because of gradient energy and the second term because of bulk energy of system. They can be calculated by $\lambda = 3\sigma\varepsilon/(2\sqrt{2})$ and $f(C) = (C^2-1)^2/(2\varepsilon)^2$ where σ denotes the interfacial tension and ε the capillary width which is a scale for interface thickness. The non-dimensional Cahn number $Cn = \varepsilon/l$ relates the interface thickness to a characteristic length l, e.g., the bubble or droplet diameter. In one dimension (1D) for a planar interface, the variation of C at equilibrium is given by

$$C = \tanh(\frac{x}{\sqrt{2}\varepsilon}) \tag{2.9}$$

If $-0.9 < C < 0.9$ is taken as the diffuse interface, then the length normal to the surface $l_C = 4.164\varepsilon$ expresses the interfacial thickness where the physical properties change rapidly but smoothly. In Fig 2.3, C is plotted against the x direction which is normal to interface. Here, $\varepsilon = 1\times10^{-5}$m and for $-0.9 < C < 0.9$, the interface thickness is $l_C = 4.164\times10^{-5}$m.

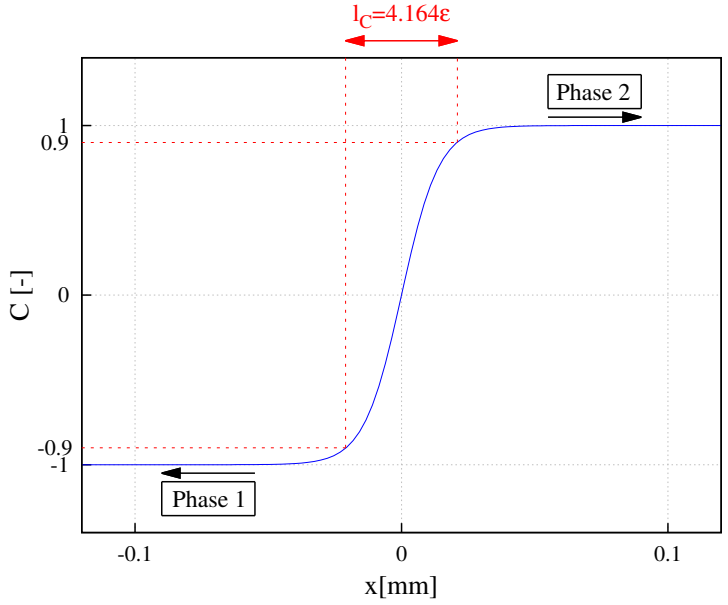

Figure 2.3.: Order parameter across the diffuse interface in the Phase Field method.

The convective Cahn-Hilliard equation, which is the modified version of Eq. (2.3) for PFF, governs the interface dynamics [23]

$$\frac{\partial C}{\partial t} + (\mathbf{U} \cdot \nabla)C = \kappa \nabla^2 \phi \tag{2.10}$$

where κ the Cahn-Hilliard mobility (diffusion parameter) and ϕ chemical potential which is the rate of change of mixing energy with respect to C, shortly $\phi = \partial \mathcal{F}/\partial C$. The Eq. (2.10) are coupled with Navier-Stokes equations in the solver *phaseFieldFoam* (PFF) in OpenFOAM-1.6-ext which uses Phase Field method. For PFF, the Eqs. (2.1) and (2.2) represent mass and momentum conservation, respectively [23]. The density and viscosity are dependent on the order parameter

$$\rho = \frac{1}{2}\left[\rho_l(1+C) + \rho_g(1-C)\right] \tag{2.11}$$

$$\mu = \frac{1}{2}\left[\mu_l(1+C) + \mu_g(1-C)\right] \tag{2.12}$$

where ρ_l and ρ_g are density of liquid and gas phases and μ_l and μ_g are their viscosities. Finally, it is important to mention that instead of CSF in IF, the surface tension force here is modelled by $\mathbf{F}_\sigma = -C\nabla\phi$ [22].

2.4. Definition of a Case in OpenFOAM

There are only text files in three directories to set up a case study in OpenFOAM. These directories are as follows: 0, *constant* and *system*. The results are also text files and written in so-called *time*-directories. In the 0-directory, the initial conditions for all boundaries are defined. In the *constant*-directory, the geometry and its boundaries together with number of mesh cells are written in the *polyMesh*-subdirectory. Physical properties and turbulence modelling as well as gravity are written in different files in the *constant*-directory. In the *system*-directory, the solver, start/end time, time step and functions for post-processing are written in *controlDict* file. Discretisation schemes, tolerances and algorithm controls for different parameters in the solution are in other files in the *system*-directory [2].

Using Cartesian coordinates in OpenFOAM, one needs to define all parameters in a three dimensional (3D) system. For two dimensional (2D) simulations, the length of domain in the third direction is regarded in the order of magnitude of one computational cell size in other directions. The focus of this work is on a 2D bubble and hence, the variations of parameters in the third direction (z) are not considered.

2.4.1. Initial and Boundary Conditions

The phases in multiphase simulations are defined by $alpha1$ in IF and C in PFF, i.e., $alpha1 = 0$, $C = -1$ represent a domain filled with air and $alpha1 = 1$, $C = 1$ stand for a domain filled with water. The cells with $0 < alpha1 < 1$ and $-1 < C < 1$ remark the interface between air and water to define an air bubble in water. Hence, it is required to define the air bubble as a circle by means of variation of $alpha1$ and C. For this purpose, a *setFieldsDict*-file in the *system*-directory in IF is applied. As can be seen in Appendix A.1, a cylinder in 3D is defined, which reduces to a circle in 2D. As seen in Fig. 2.4, there are no specific cells for interface at the beginning of simulation, i.e., the cells only with $alpha1 = 0$ or $alpha1 = 1$, but VOF causes smearing of the interface after running the simulation. To diminish this smearing, IF uses a compression term explained in section 2.2.

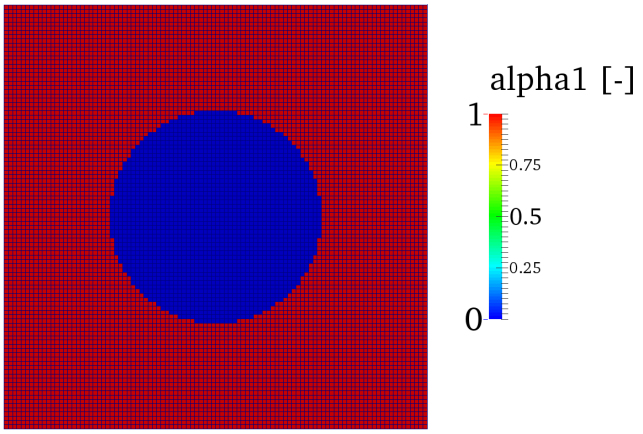

Figure 2.4.: Initial conditions for an air bubble in water in IF using rectangular cells.

Unlike in IF, the interface thickness should be defined at the beginning of the simulation in PFF using variable C with a predefined interface thickness. In other words, one of initial conditions is that the domain is partitioned into three parts: water, air and interface between them. Therefore, the *setFieldsDict*-file cannot be implemented in PFF any more for variation of C, because it is only for basic geometric shapes. For more complicated non-uniform initial condition in OpenFOAM, a developed version of *setFieldsDict*-file is necessary. This utility is $funkySetFields$ and written as a command line. Eq. (2.13) (Appendix A.2) represents how three zones using only one function are defined, which is recognisable in Fig. 2.5. This function was written for 1D in the Eq. (2.9) and the 2D version of it reads

$$C = \tanh\left\{\frac{\sqrt{(x-x_i)^2+(y-y_i)^2}-0.5D_{B,i}}{\sqrt{2}\varepsilon}\right\} \tag{2.13}$$

where x_i and y_i specify the initial spatial position of bubble centre and $D_{B,i}$ is the initial bubble diameter.

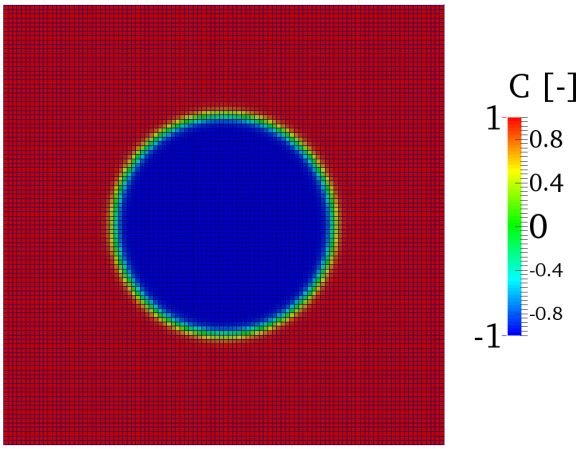

Figure 2.5.: Initial conditions for an air bubble in water in PFF on rectangular cells.

2.4.2. Temporal Resolution

In numerical simulation, one of the important non-dimensional numbers is the Courant number, Co, which is a scale for the movement of fluid in computational cells and a measure for stability of the numerical method. It is defined by

$$Co = \frac{|\mathbf{U}_{max}|\Delta t}{\Delta x} \tag{2.14}$$

where Δt is the computational time step and Δx is the mesh size. Courant numbers less than unity means that the fluid particles stay in the same cell or move through only one cell at each time step. On the other hand, with $Co > 1$, they can pass more than one cell at each time step and this can influence negatively on convergence of the numerical method. It is well-known that for multiphase simulations, Co must be lower than 1, otherwise the interface smears due to discrepancy in numerical and physical propagation of information. Therefore, for the case study here, bubble in equilibrium, the time resolution is chosen not only by the time step but also by a maximum Courant number, $maxCo$, with a value of 0.1 in *controlDict*-file. To satisfy the Courant criterion, selecting a flexible time step results in less computational cost. For this purpose, $adjustTimestep$ should be on and a value for $maxDeltaT$, which is the upper limit for the time step [2] should be specified. Shortly, it can be written that, the time step is the minimum of the Δt obtained from Co criterion and the upper limit.

$$\Delta t = min\left\{\Delta t_{maxCo},\ maxDeltaT\right\} \tag{2.15}$$

Diffusion number, D, is another non-dimensional number to be considered for the stability of the numerical method [24]. It is defined by

$$D = \frac{\Gamma \Delta t}{(\Delta x)^2} \tag{2.16}$$

where Γ is the diffusion coefficient. For two-phase flows, the higher kinematic viscosity of phases is taken as the diffusion coefficient which is in the case of an air bubble in water, the kinematic viscosity of air, ν_a, where a stands for air. It will be explained in section 3.2.2 that, this number should not exceed one, in order to obtain results which are physically reasonable. In *conterolDict*-file, dissimilar to $maxCo$, there is no option for D to be predesignated; however the resultant Δt from Eq. (2.15) is used to calculate this number.

2.5. Evaluation of Simulation Results and Related Errors

In this work, for post precessing, the utilities *sample* and $swak4foam$ in OpenFOAM are used. In the following sections, evaluation of some information with a short description of their OpenFOAM codes is discussed. To reach this target, functions can be configured in the *controlDict*-file in *system*-directory. These functions operate during the run-time and write the data in the *postProcessing*-directory.

2.5.1. Parasitic Currents

For a bubble in equilibrium, errors in discretisation and approximation of curvature cause imbalance between $\mathbf{F}_\sigma$ and ∇p in Eq. (2.2), which lead to parasitic currents, especially around the interface. Appendix A.3 expresses the evaluation of the maximum parasitic current using $swak4foam$ utility. To attain this objective, a function is defined which gives at each time step, the maximum magnitude of all velocity vectors in the whole computational domain to investigate the worst possible magnitude for this numerical error.

$$|\mathbf{U}_{max}| = max\left\{|\mathbf{U}_m| : m = 1, ..., N\right\} \tag{2.17}$$

where $m = 1, ..., N$ denote all cells in the whole computational domain. As already discussed in section 2.2, the largest parasitic currents are expected to be around the interface, what is visible in Fig. 2.6 visualised using $ParaView$ [25]. In this figure, the velocity field inside and outside of an air bubble surrounded by water is shown, which is obtained by the IF solver. Although the initial velocity is set to zero everywhere, however, because of the asymmetric large parasitic currents, the bubble is distorted, moved from its initial

place and even can exit the cyclic boundaries from one side and enter from another side in some cases.

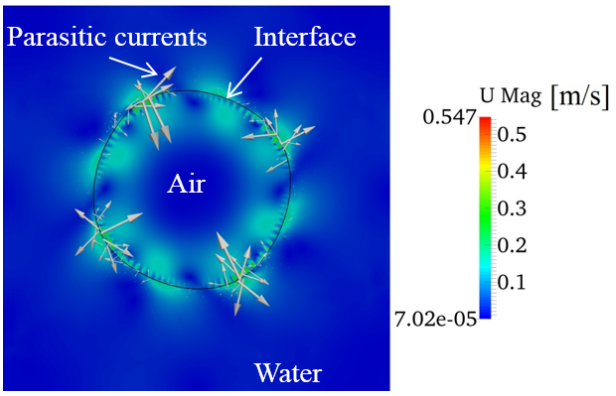

Figure 2.6.: Contour of parasitic velocity magnitude inside and outside of an air bubble using IF, initially at equilibrium, surrounded by water in a 2D domain. Visualisation is performed using *ParaView*.

Because parasitic currents show oscillatory behaviour in some simulations, they are evaluated in this thesis by averaging over last time steps where the oscillation is negligible, i.e., when the steady state is reached. For instance, in Fig. 2.7, a typical trend for the maximum parasitic velocity as s function of computational time is shown . As it is revealed, after an arbitrary time, in this case, $t = 0.3\ s$, one can assume an average terminal value for the maximum velocity.

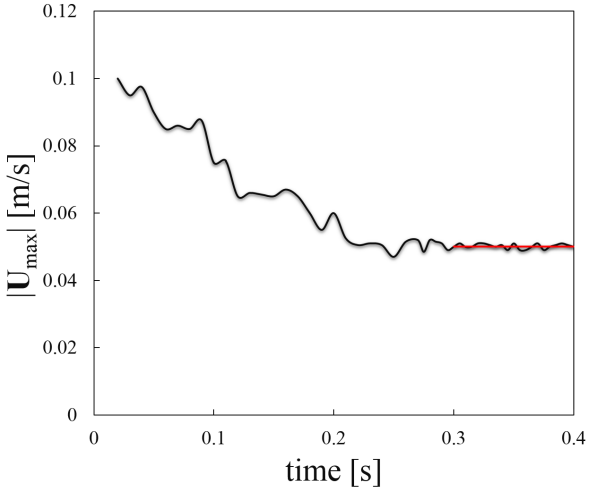

Figure 2.7.: Averaging of the maximum parasitic current because of temporal oscillation.

2.5.2. Displacement of the Bubble

Appendix A.4 describes the function that has been written to find the position of the bubble centre at each time step. The x and y positions of the bubble centre can be expressed mathematically in Eqs. (2.18) and (2.19) as

$$x_C = \frac{\sum_{m=1}^{N}(1-\alpha_m)V_m x_m}{\sum_{m=1}^{N}(1-\alpha_m)V_m} \tag{2.18}$$

$$y_C = \frac{\sum_{m=1}^{N}(1-\alpha_m)V_m y_m}{\sum_{m=1}^{N}(1-\alpha_m)V_m} \tag{2.19}$$

where V_m is the volume of each cell and calculated by $V_m = \Delta x \cdot \Delta y$. Because in this work, the equidistant orthogonal grid is used, this term can be omitted from the Eq. (2.18) and (2.19). The displacement of the bubble is then equal to the distance between two positions of bubble centre at two consecutive time steps, that is, $x_D = \sqrt{x_C^2 + y_C^2}$. In sections 3.1 and 3.2, the influence of solvers and different numerical and physical parameters on the parasitic currents and bubble displacement will be discussed in more detail.

2.5.3. Interface Thickness and Bubble Diameter

The interface thickness is of interest in this study, since it is one of the important parameters in characterisation of parasitic currents as well as in capturing the physics. The thinner the interface, the more accurate the results of numerical simulations in estimating the physics. However, steeper gradients of physical properties, such as viscosity and density for thinner interfaces result in larger parasitic velocities. Thus, a compromise in selecting the bubble interface is a necessity. This, requires a numerical study of the effect of interface on the fluid dynamics in the model. Appendix A.5 explains how a function can take all points with an equal value of a parameter (such as $alpha1$ in IF and C in PFF) and build a surface from these points in 3D (a curve in 2D). Because of this feature, it is called $isoSurface$ in OpenFOAM. Fig. 2.8 exhibits schematically an air bubble in water in IF with three circles deduced from $isoSurface$. The distances between inner circle with $alpha1 = 0.1$ and outer circle with $alpha1 = 0.9$ gives the interface thickness, which means as delimiters for the interface, the values 0.1 and 0.9 are chosen. In this work, four points on x axis gives two values for the interface thickness ($x_5 - x_1$ and $x_3 - x_7$ in Fig. 2.8), the same from four points on y axis ($y_6 - y_2$ and $y_4 - y_8$ in Fig. 2.8). The average of these four values is considered as the interface thickness. On the middle circle, $alpha1 = 0.5$ and twice of the average of distances of all points on this circle from the centre of bubble results in the mean bubble diameter D_B. The related error for the diameter is standard deviation (STD) which helps to understand how the bubble shape deviates from a perfect circle.

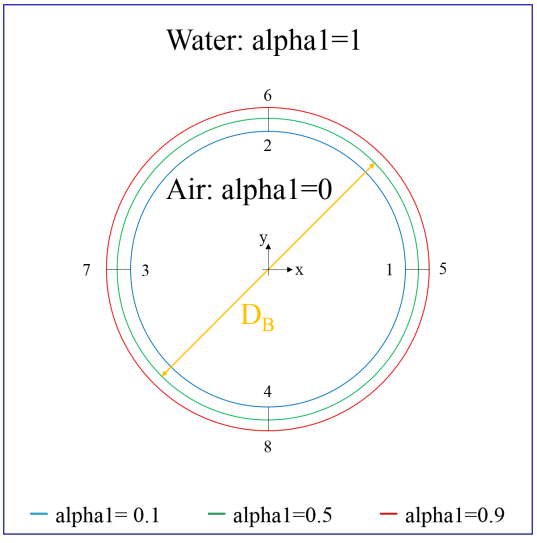

Figure 2.8.: Schematic illustration of $isoSurface$ in IF for the bubble in equilibrium.

In a similar manner, the interface thickness and the mean bubble diameter is defined in PFF by using $C = -0.9$, 0 and 0.9. In this work, the analytical solution for a circle interface of bubble in equilibrium is approximated by the analytical solution of a planar interface. In section 2.3, it was explained that for $-0.9 < C < 0.9$, the length of interface is $l_C = 4.164\varepsilon$ in a Phase Field method. Therefore, if the initial bubble diameter is resolved

by $N_B = D_B/\Delta x$ where D_B is the bubble diameter and Δx the mesh size in x direction, then by taking $L = D_B$ in the definition of Cahn number, the corresponding grid resolution for the diffuse interface thickness can be calculated by [23]

$$N_C \approx 4\frac{\varepsilon}{\Delta x} = 4\frac{Cn \cdot D_B}{\Delta x} = 4Cn \cdot N_B \tag{2.20}$$

Here, $C = 0$ is used to determine the mean bubble diameter.

2.5.4. Average Pressure Difference

To verify the accuracy of the simulation results, comparison between the theoretical prediction and numerical simulation of the pressure difference between inside and outside of the bubble is conducted. For this purpose, in the simulations an average value is required for pressure in both phases. To calculate the average pressure difference between the air bubble and water, it is required to subtract the outcomes of two functions reported in Appendix A.6. The routine is to make a condition by means of an arbitrary threshold. If this condition for a cell is fulfilled, then its information (pressure and volume) will be taken. In cells where $alpha1 > 0.99$ in IF or $C > 0.98$ in PFF, $j = 1, ..., N_w$, the pressure and volume come into account to reckon the average pressure of water, $p_{avg,w}$ where w is the abbreviation of water

$$p_{avg,w} = \frac{\sum_{j=1}^{N_w} p_j V_j x_j}{\sum_{j=1}^{N_w} V_j} \tag{2.21}$$

Analogue for cells with $alpha1 < 0.01$ in IF or $C < -0.98$ in PFF, $k = 1, ..., N_a$, to calculate the average pressure of inside the air bubble $p_{avg,a}$

$$p_{avg,a} = \frac{\sum_{k=1}^{N_a} p_k V_k x_k}{\sum_{k=1}^{N_a} V_k} \tag{2.22}$$

From Eqs. (2.21) and (2.22), the average pressure difference

$$\Delta p_{numerical} = p_{avg,a} - p_{avg,w} \tag{2.23}$$

and its relative error

$$\varepsilon_p = \left| \frac{\Delta p_{numerical} - \Delta p_{analytical}}{\Delta p_{analytical}} \right| \tag{2.24}$$

can be written, where $\Delta p_{analytical}$ derives from Young-Laplace equation, which in 2D for the air bubble in water, is [3]

$$\Delta p_{analytical} = \frac{2\sigma}{D_{B,\ analytical}} \tag{2.25}$$

where $D_{B,\ analytical}$ is the analytical (initial) bubble diameter.

3. Bubble in Equilibrium

This chapter presents the comparison of two introduced methods, VOF and Phase Field methods implemented in OpenFOAM whereby VOF solver is IF and Phase Field solver is PFF. A case study, which is a static air bubble in stagnant water using IF and PFF solvers will be described. The density ratio of water and air is high and this makes the case study more critical than a case, such as with water and oil. Moreover, the small diameter of the bubble lead to the problematic capillary numbers. The bubble in equilibrium is a 3D case study and in this thesis, for simplicity, a 2D circle, corresponding to an infinitely stretched cylinder is simulated with the initial velocity of zero and without gravity field. The motion of such a bubble is simulated to determine the parasitic currents.

3.1. Comparison with Test Cases from Literature

Before the results for an air bubble in micro scale is presented, it is meaningful to start with two relatively easier case studies from literature. The goal is to compare the results of IF and PFF with other authors' findings. The first case study is chosen because the density and viscosity ratios of two phases are equal to 1. It prevents from any possible influence of different densities or viscosities of phases on the numerical results. The simplicity of the second case, which is a simulation of a droplet in air, is because of its large scale and this circumstance that only one time step is simulated.

3.1.1. Albadawi's Case

Albadawi et al. [13] simulated in IF the 2D stationary bubble with the diameter of 1 cm under zero gravity where the density and viscosity ratios assumed to be 1 ($\rho_l/\rho_g = 1$ and $\mu_l/\mu_g = 1$). Popinet et al. [26] implemented this case study in order to affirm that for a wide range of the non-dimensional Ohnesorge number, $Oh = \mu_l/(\sigma\rho_l D_B)^{0.5}$, the spurious currents are linear proportional to σ/μ. In other words, for an arbitrary invariant Oh, the non-dimensional capillary number $Ca = \frac{|\mathbf{U}_{max}|}{\sigma/\mu}$ is constant which means that the relative effect of viscous and surface tension forces on the interface is constant and independent on the mesh. Albadawi et al. [13] set $Oh = 0.0316$ and varied the grid resolution from 50×50 to 500×500, which means that the number of cells for bubble N_B is 10 to 100. Their time step was defined by $\Delta t = 0.1\Delta x$ and the end time of the simulation was 0.1 s. They reported that they observed the same results with $Co = 0.1$ using the adaptive time stepping.

In this work, Albadawi's case study is replicated by means of IF and PFF with $\nu_l = \nu_g = 0.001$ m$^2\cdot$ s^{-1}. In Fig. 3.1, the capillary number is plotted at different grid resolutions for the bubble. For convenience, the Δx equivalent to N_B is shown at the top horizontal axis, which corresponds the mesh sizes (the bottom horizontal axis). Although Albadawi et al. [13] used IF and showed an almost constant Ca number as it was expected. The Ca numbers in this study using IF are not quantitatively identical with their results. A possible reason can be the different OpenFOAM versions. Nevertheless, none of them show the convergence with mesh refinement which is in agreement with the results by Popinet et al. [26].

Cai et al. [23] recognised if the interface in PFF is resolved by at least six mesh cells, then the numerical results do not depend on N_C any more. Here, N_C is chosen from 4 to 8 and to see the influence of density, two different values are given in PFF. PFF shows the decreasing trends of Ca for both values of density which means that the maximum parasitic current is not linearly proportional to the surface tension to the viscosity ratio and finer meshes result in the lower parasitic currents. The curves are compared with the 1$^{\text{st}}$ and 2$^{\text{nd}}$ order decreasing trends. For $\rho_l = \rho_g = 1000$ kg $\cdot$ m^{-3} can be seen that the variation in capillary number obeys the 2$^{\text{nd}}$ order decreasing convergence trend.

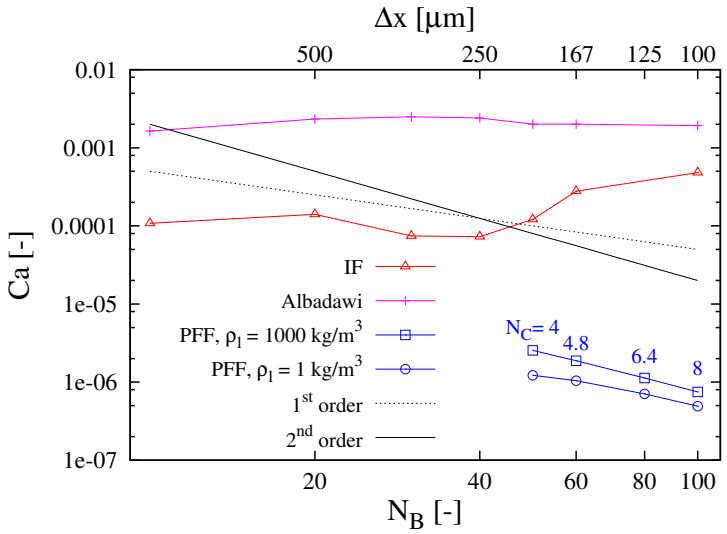

Figure 3.1.: Comparison of the terminal capillary number in IF and PFF with Albadawi's results for the air bubble in water in equilibrium with $\rho_l/\rho_g = 1$, $\mu_l/\mu_g = 1$ and $Oh = 0.0316$.

3.1.2. Yokoi's Case

To minimise the parasitic currents in multiphase simulations such as capturing of droplet splashing, Yokoi [11] on the basis of study by Francois et al. [8] offered a numerical method, namely, the level set based density-scaled balanced CSF model. Previous researches [8, 9, 27] showed that the density scaling causes higher stability in calculation of the surface tension force because it shifts the smoothed symmetrical δ function of CSF model to a higher density region. The difference between CSF and balanced CSF models is in their discretisation schemes. In the balanced CSF model, $\nabla\alpha$ in $\mathbf{f}_\sigma = \sigma\mathcal{K}\nabla\alpha$ and ∇p in the projection step should be discretised by the same strategy.

As a verification case study for his proposed numerical framework, Yokoi [11] simulated a droplet in air in equilibrium with a diameter $D_D = 2$ m, the liquid density $\rho_l = 1$ kg $\cdot$ m^{-3}, the air density $\rho_g = 0.001$ kg $\cdot$ m^{-3} and the surface tension coefficient $\sigma = 1$ kg $\cdot$ s^{-2}. In

this thesis, his case is simulated by IF and PFF in order to compare the results of different numerical methods only after one time step which is 1 μs. Because he assumed that the liquid is inviscid, due to not having the numerical corruption, ν_l and ν_g in IF and PFF is given 10^{-40} $\mathrm{m}^2 \cdot \mathrm{s}^{-1}$, which is not exactly zero, but is an acceptable value for this assumption. The 2D computational domain is a 4 m×4 m square and a rectangular Cartesian grid is created on this domain for discretisation.

Fig. 3.2 illustrates the comparison between Yokoi's results and the outcomes of IF and PFF. This comparison is represented as a convergence study on the maximum parasitic current. As can be seen in Fig. 3.2(a), IF like standard CSF model and density-scaled CSF model present no convergence with grid refinement. On the contrary, the maximum parasitic current shows the monotonically decreasing curves by PFF, the balanced CSF and density-scaled balanced CSF models in Fig. 3.2(b). The two latter models show the 2$^{\mathrm{nd}}$ order of decreasing trend. This trend changes into a 1$^{\mathrm{st}}$ order one, when mesh refinement is implemented. On the other hand, for the same range of mesh size where the two models cannot eliminate the parasitic current rapidly, PFF diminishes it by 2$^{\mathrm{nd}}$ order. Therefore, one can conclude that PFF is more suitable in damping this numerical error, when finer grids are implemented.

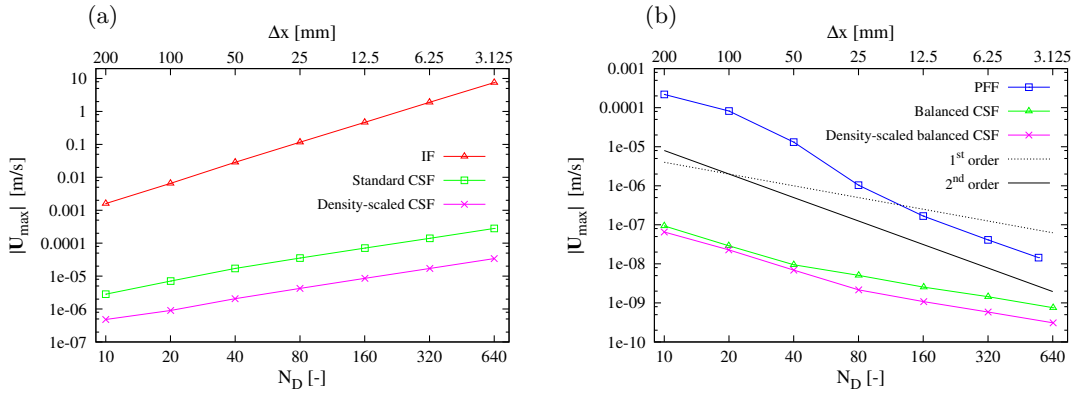

Figure 3.2.: Comparison of the maximum parasitic current in (a) IF and (b) PFF with Yokoi's results after one time step for an inviscid static droplet in equilibrium with $\rho_l = 1$ kg $\cdot$ m^{-3}, $\rho_g = 0.001$ kg $\cdot$ m^{-3} and $\Delta t = 1$ μs.

3.2. A Sub-millimetre Air Bubble in Water

The previous case studies on the comparison of different solvers with other results in literature, brought the knowledge that PFF can plausibly deal with the problem of parasitic currents. The next case study, which is of interest to FESTO AG. & Co. KG, is a 2D simulation of a motionless air bubble in stagnant water in micro scales. The computational domain is defined as 1000 μm × 1000 μm × 1 μm. The gas phase is initialised in the form of a circle ($D_B = 500$ μm) in the centre of the domain, surrounded by the liquid phase for the rest of the domain. This means that the length of the domain, l, in each direction (x and y in Cartesian coordinates) is twice the bubble diameter, D_B.

$$\frac{l}{D_B} = 2 \tag{3.1}$$

All four boundary conditions are defined as cyclic. The time step is selected by checking the criterion $maxCo = 0.1$ to find a value for Δt and comparing it with $maxDeltaT = 5$ μs.

The physical properties are as follows:

1. Density:

   i) air: $\rho_a = 1.2$ kg $\cdot$ m^{-3} ii) water: $\rho_w = 997$ kg $\cdot$ m^{-3}

2. Kinematic Viscosity:

   i) air: $\nu_a = 1.531 \times 10^{-5}$ m$^2 \cdot$ s^{-1} ii) water: $\nu_w = 1 \times 10^{-6}$ m$^2 \cdot$ s^{-1}

3. Surface tension coefficient: $\sigma = 0.07286$ kg $\cdot$ s^{-2}

In the following sections, the effects of numerical parameters on the results of simulations using IF and PFF based on the study in Cai et al. [23] will be presented. These parameters are: mesh resolution Δx, Cahn number Cn, temporal resolution Δt, Cahn-Hilliard mobility κ and bubble Diameter D_B.

3.2.1. Influence of the Mesh Resolution

The domain inside the bubble is discretised with 25, 50, 75 and 100 quadrilateral cells in both x and y directions on the main diameter. According to Eq. 3.1, the whole computational domain is discretised with 50, 100, 150 and 200 quadrilateral cells in both x and y directions. Fig. 3.3 shows the time evolution of the maximum parasitic current and the non-dimensional displacement of the centre of bubble for both solvers. The steady state values of these parameters are required for evaluating the accuracy of both solvers in predicting parasitic currents. Therefore, the time evolution of them is studied at the first step. Initially, the end time of the simulations was set as 0.15 s and after that as 0.2 s; both were unsuccessful in providing a steady state solution. Finally, the simulation time is assumed as 0.4 s to reach a steady state solution for both solvers. This value remained fix for all cases throughout this thesis. For temporal resolution, $maxDeltaT = 5$ μs and $maxCo = 0.1$ are chosen. Jacqmin [6] stated that $\kappa \approx O(\varepsilon^2)$ which is the formulation for the mobility factor as a function of capillary width. Here, $\kappa = G_\kappa \varepsilon^2$ where G_κ is chosen as a constant value and equal to 0.1 m $\cdot$ s $\cdot$ kg^{-1} to ensure the stability of PFF.

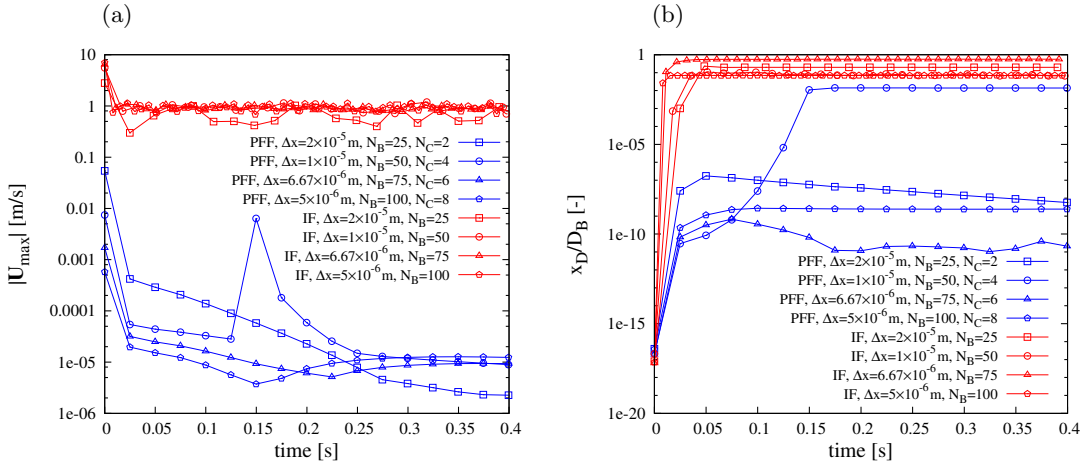

Figure 3.3.: Time evolution of (a) the maximum parasitic current and (b) the non-dimensional displacement of centre of bubble in IF and PFF with $D_B = 500$ μm, $Cn = 0.02$, $\varepsilon = 10$ μm and $\kappa = 1 \times 10^{-11}$ m$^3 \cdot$ s $\cdot$ kg^{-1}.

As mentioned previously, the maximum velocity here in Fig. 3.3(a) is defined as the maximum magnitude of velocity in the domain. The non-dimensional displacement in Fig. 3.3(b) is obtained by dividing the total displacement of the centre of bubble to its initial diameter. Although the two figures are not related directly to each other, they should be analysed simultaneously, because the more the bubble moves, the higher is the velocity magnitude of the induced parasitic flow in the domain. As can be seen in Fig. 3.3(a), the IF solver is not accurate in predicting the maximum parasitic current, regardless of the mesh resolution. The maximum magnitude of parasitic currents reaches to a value of approximately 1 m $\cdot$ s^{-1} for all of the mesh sizes in the steady state. The displacement

of the centre of bubble is not the same for all cases and varies from almost 10% of D_B for the cases with $N_B = 50, 100$ to ca. 70% of D_B for $N_B = 75$ in the steady state. Apparently, in the scale of microfluidic devices, since the flow is not dominated by inertia and consequently the non-dimensional Weber number, ratio of inertia to surface tension forces [3], is not large, the solver is not capable of damping the parasitic currents. The accuracy of IF at high Weber numbers, however, is reported elsewhere [12, 28, 29, 30].

The PFF solver, on the other hand, shows a different behaviour to IF as a function of the mesh size. Firstly, to reach a plateau, the solver requires longer simulation time compared to IF. Secondly, the maximum parasitic current and the displacement of the centre of bubble are orders of magnitude smaller than the data obtained by IF. As can be seen in the graphs, the maximum parasitic current approaches 10 $\mu\text{m} \cdot \text{s}^{-1}$ for all cases. Furthermore, the dimensionless bubble displacement is in the order of $10^{-8} - 10^{-10}$ times of the bubble diameter, for all cases, expect for the grid with $N_B = 50$, whose terminal displacement is almost 1% of the bubble diameter. In the latter case, a jump in the parasitic velocity magnitude as well as the displacement is observed at time $t = 0.15$ s. This numerical effect is a consequence of the few number of cells adopted to capture the interface which is shown as parameter N_C in the graphs. According to Cai et al. [23], the PFF solver is not suitable for simulations with $N_C < 4$ and the same conclusion can be derived from the results presented in this work. Therefore, the results obtained with $N_B = 75, 100$ which correspond to $N_C = 6,\ 8$ respectively, at a constant Cahn number $Cn = 0.02$ are reliable and clearly show that the PFF solver is successful in predicting the state of the bubble with negligible parasitic currents.

Of interest, is the magnitude of the change of the maximum terminal parasitic velocity obtained from the two solvers as a function of the mesh size. This is plotted in Fig. 3.4. As can be seen, PFF predicts the maximum velocity almost five orders of magnitude less that IF, for all of the resolutions. Moreover, for both solvers, the velocity magnitude is approximately independent of the mesh size. As discussed before, the results obtained from the cases with $N_C = 2,\ 4$ are not reliable. Therefore, the increasing trend in the velocity magnitude is not conclusive. The two curves are also compared with the 1st and 2nd order decreasing trends. It can be seen that the spurious currents do not obey the decreasing convergence trends. Therefore, in the range of the mesh resolution investigated in this study, it is concluded that PFF is very successful in reduction of parasitic currents from the numerical simulation.

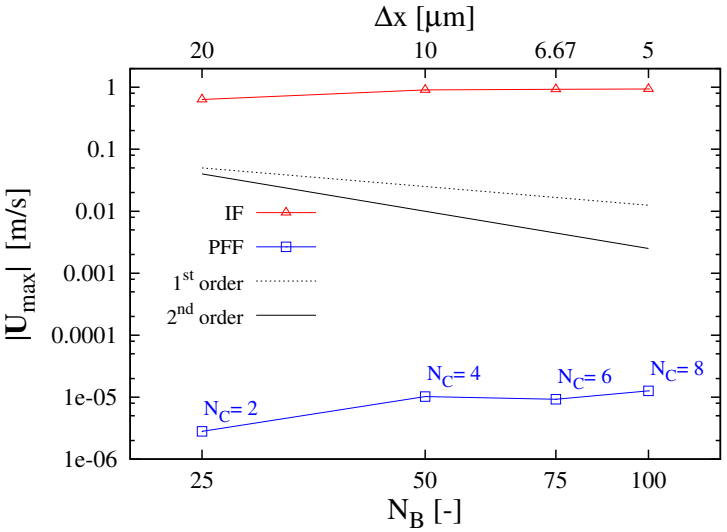

Figure 3.4.: Terminal magnitude of the maximum parasitic current in IF and PFF with $D_B = 500\ \mu\text{m},\ Cn = 0.02,\ \varepsilon = 10\ \mu\text{m}$ and $\kappa = 1 \times 10^{-11}\ \text{m}^3 \cdot \text{s} \cdot \text{kg}^{-1}$.

From this conclusion and also the results of sections 3.1.1 and 3.1.2, it is worthwhile to mention that for $\rho_l = \rho_g$ and $\mu_l = \mu_g$, PFF shows convergence with mesh refinement, while for air-water system this cannot be achieved for the air bubble in water. If there is a large scale water droplet in air, then PFF shows convergence.

To investigate the effect of mesh size on the accuracy of the solvers in interface capturing, the phase fraction $alpha1$ for IF and the order parameter for phase identification C for PFF are plotted along the horizontal diameter of the bubble in Fig. 3.5 by means of OpenFOAM sample utility. For comparison, the theoretical value is also shown. As can be seen from Fig. 3.5(a), the interface between gas and liquid is captured with considerable numerical diffusion, especially for coarser grids. This numerical diffusion is sufficiently small when the number of grid increases and for $N_B = 100$, the difference between theoretical curve and numerical prediction is quite small. For PFF, since the Cn number is fixed, the interface thickness is given the same for all of the simulations. As can be seen from Fig. 3.5(b), by increasing N_B and correspondingly N_C, all of the curves predict the interface thickness close to the theoretical value of the interface thickness which is 4.164ε.

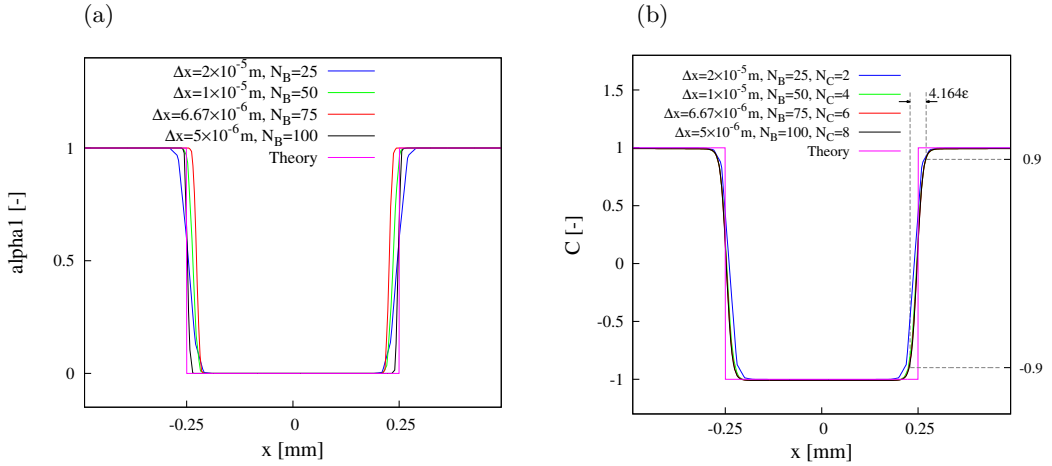

Figure 3.5.: Terminal phase distribution along the horizontal diameter of bubble in (a) IF and (b) PFF with $D_B = 500$ μm, $Cn = 0.02$, $\varepsilon = 10$ μm and $\kappa = 1 \times 10^{-11}$ $\mathrm{m}^3 \cdot \mathrm{s} \cdot \mathrm{kg}^{-1}$.

The results for verification of the average pressure difference obtained from IF and PFF are shown in Fig. 3.6. From Eq. (2.25), this value is calculated as $\Delta p = 291$Pa. For simulations, an averaging on pressure over both liquid and gas domains is performed discussed in 2.5.4. The relative error of pressure estimation is also reported. As can be seen, the pressure difference cannot be estimated accurately by IF, even with the finest resolution. The relative error between numerical and analytical predictions is ca. 10% and almost similar for all of the values of N_B. By putting this verification besides the accuracy of IF solver in interface capturing and parasitic currents, one can conclude that the solver is not precise enough in predicting a reasonable physics for a bubble in a microfluidic channel. In contrast to IF, the PFF solver is able to estimate the pressure difference with a reasonable error at higher values of N_C, as illustrated in the Fig. 3.6(b). Although the interface is diffusive here as well, the relative error between the numerical and analytical predictions is less than 1%. It is worth mentioning that the 1^{st} and 2^{nd} order decreasing convergence trend vs. grid size is not observed in the relative error obtained by both solvers.

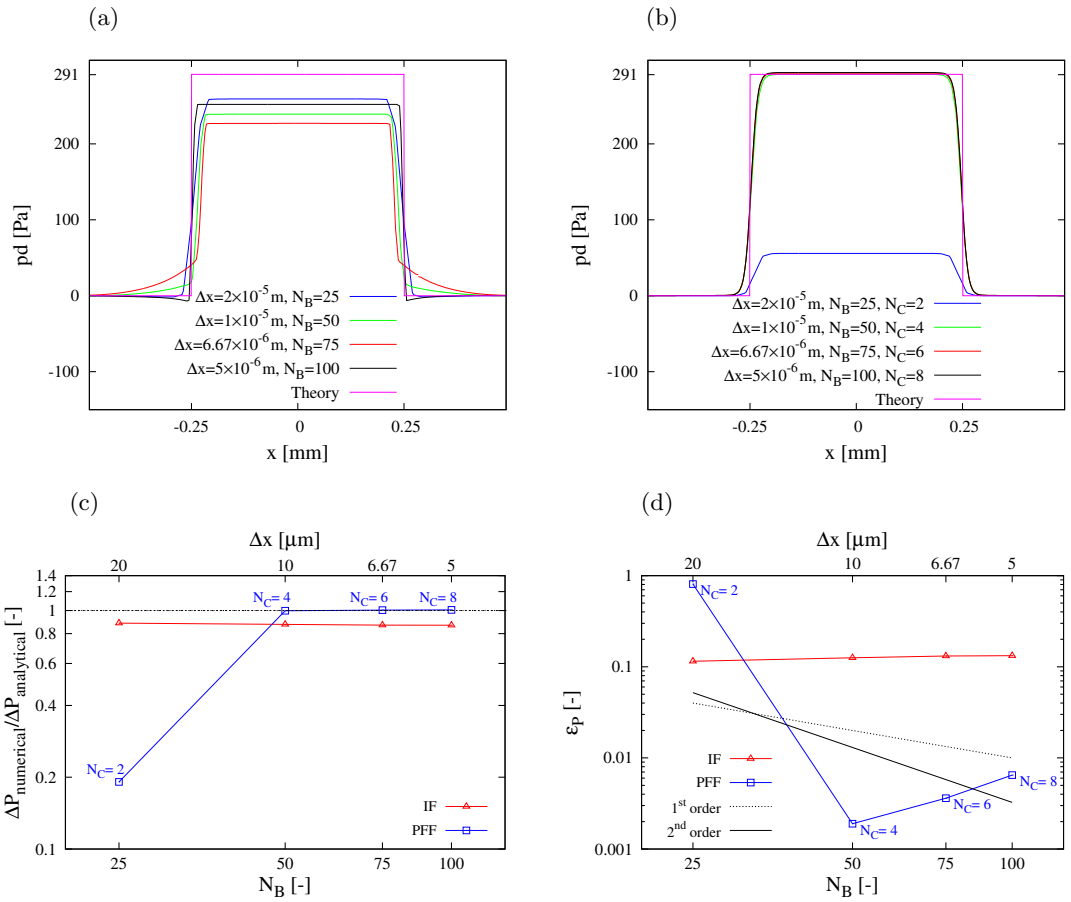

Figure 3.6.: Terminal pressure distribution along the horizontal diameter of the bubble in (a) IF and (b) PFF. (c) The non-dimensional terminal difference between the average pressures of the air bubble and water in IF and PFF and (d) its relative error where the exact value comes from Young-Laplace Eq. with $D_B = 500\ \mu$m, $Cn = 0.02$, $\varepsilon = 10\ \mu$m and $\kappa = 1 \times 10^{-11}\ \mathrm{m}^3 \cdot \mathrm{s} \cdot \mathrm{kg}^{-1}$.

The effect of mesh resolution on estimating the terminal bubble diameter is shown in Fig. 3.7. For comparison, the non-dimensional standard deviation (STD) of the calculation is also reported.

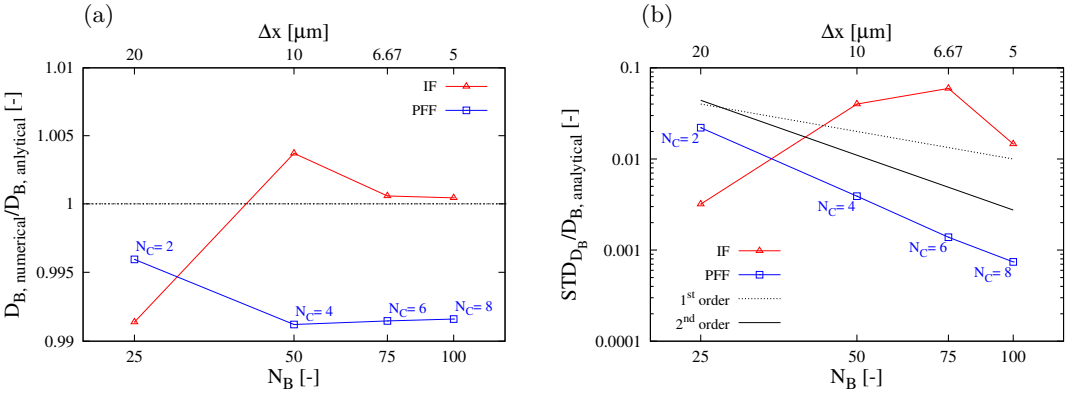

Figure 3.7.: Comparison of (a) the terminal bubble diameter in IF with PFF and (b) its non-dimensional STD with $D_B = 500\ \mu$m, $Cn = 0.02$, $\varepsilon = 10\ \mu$m and $\kappa = 1 \times 10^{-11}\ \mathrm{m}^3 \cdot \mathrm{s} \cdot \mathrm{kg}^{-1}$.

Both solvers predict the diameter of the bubble with small relative error (less than 1%). The corresponding error for IF is smaller than the one predicted by PFF. In addition,

for IF, the error is sensitive to the mesh resolution and decreases by refining the mesh size. On the other hand, the relative error of PFF is independent of the mesh size and is bigger than the one for IF. It should be noted that IF predicts the terminal diameter of the bubble bigger than its equilibrium size whereas PFF estimates a smaller bubble. The reason of this shrinkage in bubble size using PFF solver will be discussed later in section 3.2.2.

Comparison of the STD of the bubble diameter, shows that the accuracy of PFF in predicting the sphericity of the bubble increases with mesh refinement and correspondingly higher N_C and the solver is more accurate compared to 1^{st} and 2^{nd} order convergence trends. By contrast, the STD for IF becomes larger at finer grid sizes up to $N_B = 75$ and decreases again for $N_B = 100$. This is in correspondence to the maximum terminal velocity for parasitic currents, which consequently changes the shape of the interface from perfect circle. There is no dependency in the change of STD on the grid size, which shows the variance and strong asymmetry in the fluctuation around the interface. Although the STD in IF is higher than STD in PFF for $N_B = 50, 75$ and 100 and this means that the bubble distorts in IF more than in PFF, the bubble diameter (calculated by averaging, see section 2.5.3) is more accurate in IF. Fig. 3.8 reflects different concepts of both methods. In IF, the captured interface thickness is related to the grid size, therefore, it decreases with mesh refinement and varies in a 1^{st} trend with the grid resolution and its magnitude reduces to below 10 μm for $N_B = 100$ shown in 3.8(a). In PFF, however, the interface thickness is finite and determined by Cn number which is here set as a fixed number and its magnitude shows a very slow decreasing trend as a function of the grid size. In greater detail, this trend is magnified and showed as the non-dimensional thickness in Fig. 3.8(b). It can be concluded that the solver can predict the thickness close to the analytical value obtained from planar approximation, which is explained in section 2.3, when the interface is resolved with more mesh cells. As discussed before, the results obtained for $N_C = 2$ and $N_C = 4$ are not reliable, however, they are reported here to show the decreasing trend of the error.

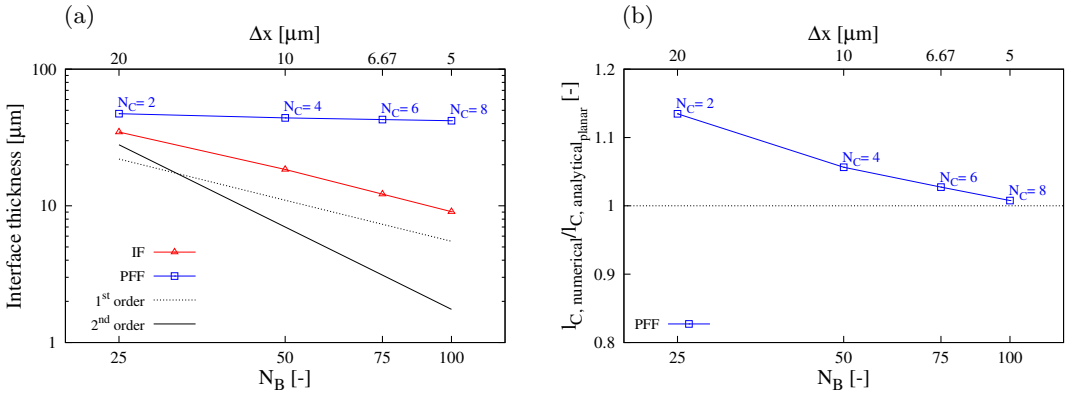

Figure 3.8.: (a) Comparison of the terminal interface thickness in IF with PFF. (b) The non-dimensional terminal interface thickness in PFF with $D_B = 500$ μm, $Cn = 0.02$, $\varepsilon = 10$ μm and $\kappa = 1 \times 10^{-11}$ m$^3 \cdot$ s $\cdot$ kg^{-1}.

3.2.2. Influence of the Cahn Number and the Temporal Resolution

After investigating the effect of mesh resolution on both IF and PFF solvers and concluding that PFF is more accurate in predicting the relevant parameters for $N_C > 4$, in this section, the effect of different Cn numbers on the physics of the bubble in equilibrium is presented. According to Eq. (2.15), here $\Delta t = min\{\Delta t_{maxCo=0.1},\ 5\mu s\}$. Here, $\kappa = G_\kappa \varepsilon^2$ with $G_\kappa = 0.1$ m $\cdot$ s $\cdot$ kg^{-1} is adopted. For all cases, $N_C = 8$ is set, which according to the results of the previous section, provides the smallest parasitic currents.

Figure 3.9 shows the time evolution of the maximum parasitic current and the non-dimensional displacement of centre of bubble at different Cn numbers. As it has been depicted by Fig. 3.9(a), the maximum parasitic velocity for the two cases of $Cn = 0.02$ and 0.04 does not exceed 0.0001 $\mathrm{m \cdot s^{-1}}$ which is quite small and therefore, the displacement of the centre of bubble is negligible, as shown in Fig 3.9(b). For $Cn = 0.01$, the maximum parasitic velocity approaches 0.1 $\mathrm{m \cdot s^{-1}}$ and hence, the bubble moves more compared to the other two cases. This analysis mean that, although the mesh inside the bubble is refined to keep N_C constant and also the interface thickness reduces at smaller Cn numbers, the parasitic velocity as well as the bubble motion is predicted less accurately. This result is not expected, since the smaller the Cn number, the more computational cost is required for the simulations.

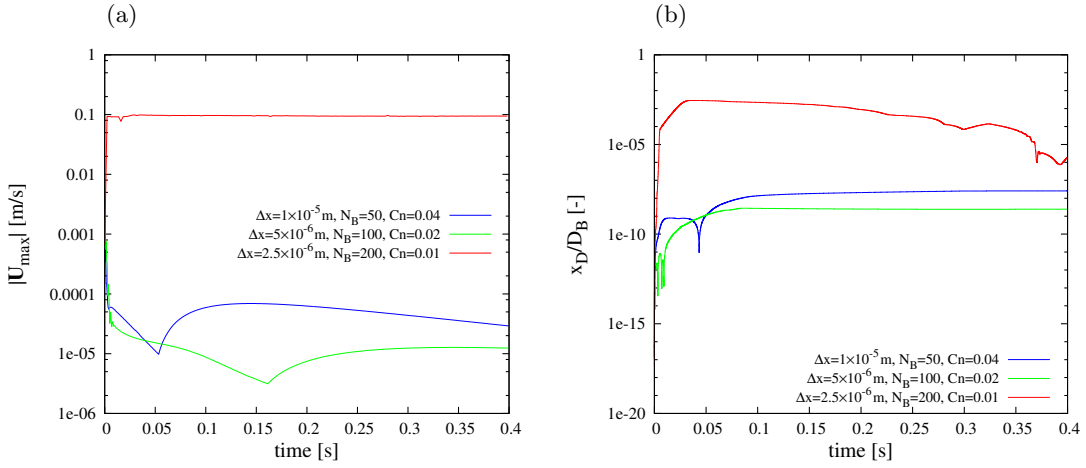

Figure 3.9.: Influence of the Cn number on the time evolution of (a) the maximum parasitic current and (b) the non-dimensional displacement of centre of bubble in PFF featuring varied κ with $D_B = 500$ μm, $N_C = 8$, $\varepsilon = Cn \cdot D_B$, $\kappa = G_\kappa \varepsilon^2$ and $G_\kappa = 0.1$ $\mathrm{m \cdot s \cdot kg^{-1}}$.

However, decreasing the Cn number leads to a better prediction of the pressure difference between inside and outside of the bubble as well as the interface thickness, as is shown in Fig. 3.10. Comparison of the theoretical prediction of the pressure difference and phase distribution with numerical results reveals that the case with $Cn = 0.01$ provides the best results with minimum numerical diffusion because Cn number is a scale for the interface thickness.

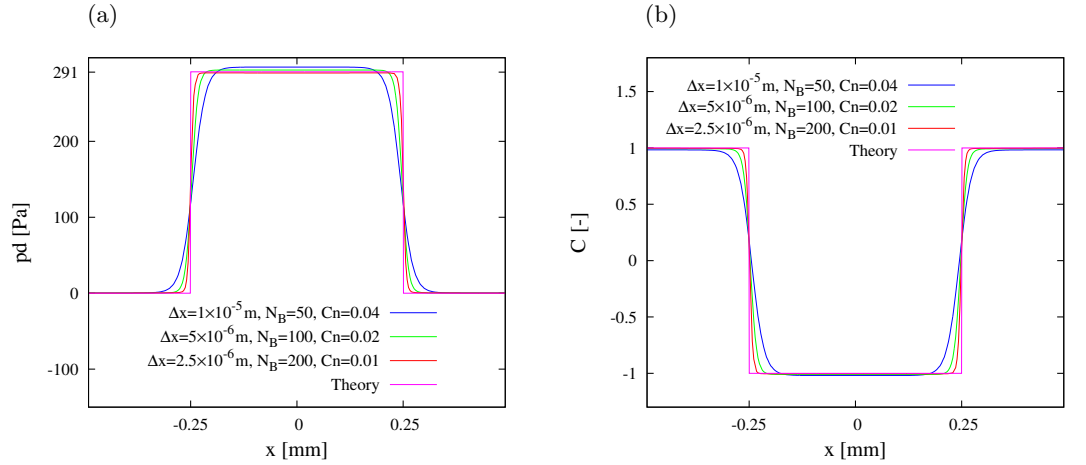

Figure 3.10.: Influence of the Cn number on the (a) pressure and (b) phase distribution along the horizontal diameter of bubble in PFF featuring varied κ with $D_B = 500$ μm, $N_C = 8$, $\varepsilon = Cn \cdot D_B$, $\kappa = G_\kappa \varepsilon^2$ and $G_\kappa = 0.1$ $\mathrm{m \cdot s \cdot kg^{-1}}$.

From the two latter parts of the analysis, one might attempt to conclude that, to reduce the parasitic currents, the Cn number should increase and to capture the interface and pressure difference more accurately, the Cn number should decrease. Thus, one might think of a Cn number that lies among the investigated values to compromise the pros and cons of the solver. Before finding a Cn number, one also may think of the effect of variable mobility as $\kappa = G_\kappa \varepsilon^2$ on the results, since by increasing the Cn, κ increases and one expects more diffusion in the results. To investigate the sensitivity of this analysis on variable κ, the same simulation is performed using a constant value of $\kappa = 2.5 \times 10^{-12} \mathrm{m}^3 \cdot \mathrm{s} \cdot \mathrm{kg}^{-1}$, which corresponds to the value of variable κ for $Cn = 0.01$. The results as the time evolution of the maximum parasitic current and the non-dimensional displacement of centre of bubble are shown in Fig. 3.11. Although there is a change in the time evolution in both curves, the steady states of the parameters are very similar to the previous case (Fig. 3.9). Hence, it is concluded that the increased level of diffusion in the results of higher Cn number is not an influence of variable formulation for κ.

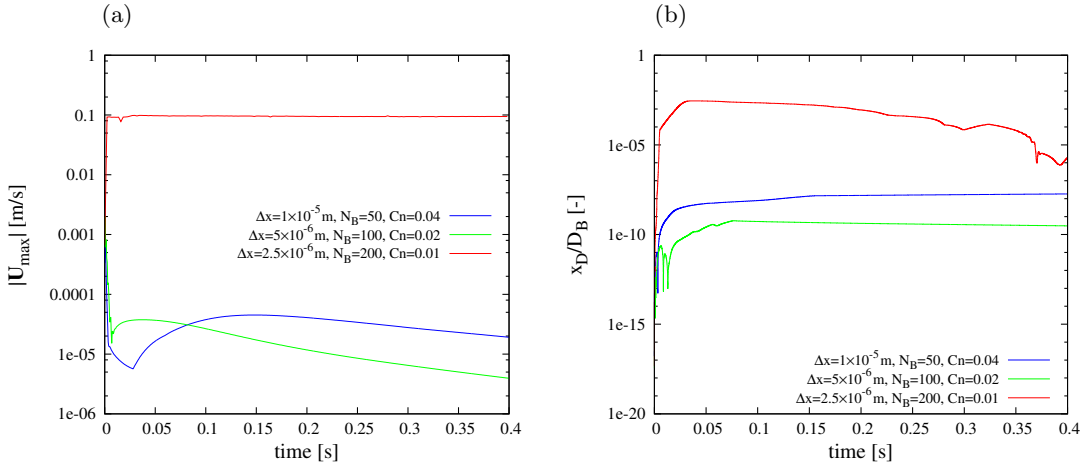

Figure 3.11.: Influence of the Cn number on the time evolution of (a) the maximum parasitic current and (b) the non-dimensional displacement of centre of bubble in PFF featuring constant κ with $D_B = 500$ μm, $N_C = 8$ and $\kappa = 2.5 \times 10^{-12} \mathrm{m}^3 \cdot \mathrm{s} \cdot \mathrm{kg}^{-1}$.

The next step of finding the suitable set of parameters will be finding a Cn number, which takes the advantages of reduced parasitic currents at higher Cn numbers and more accurate capturing of the interface and pressure difference at lower Cn numbers. Here a value of $Cn = 0.016$ is selected. To investigate the effect of diffusion, the diffusion number, D is calculated for all of the selected Cn numbers and the relative information are reported in Table 3.1. As can be seen, with the same Cn number as 0.016, the diffusion number changes from 3.56 to 0.478 when the time step from Eq. (2.15) varies from 3.72 μs to 0.5 μs when the $maxDeltaT$ alters from 5 μs to 0.5 μs. This is a very important outcome, which indicates the sensitivity of the PFF to time step itself and not only the dimensionless groups of numerical parameters.

Table 3.1.: Diffusion number, (D), in PFF with $D_B = 500$ μm, $N_C = 8$, $\varepsilon = Cn \cdot D_B$ and $\kappa = 2.5 \times 10^{-12} \mathrm{m}^3 \cdot \mathrm{s} \cdot \mathrm{kg}^{-1}$.

$Nr.$	$Cn[-]$	$\varepsilon[\mu\mathrm{m}]$	$N_B[-]$	$T_n[-]$	$\triangle x[\mu\mathrm{m}]$	$\triangle t[\mu\mathrm{s}]$	$D[-]$
1	0.01	5	200	400	2.5	1.98	4.85
2	0.016	8	125	250	4	3.72	3.56
3	0.016	8	125	250	4	0.5	0.478
4	0.02	10	100	200	5	5	3.06
5	0.04	20	50	100	1	5	0.766

To illustrate the influence of diffusion number via change of time step, the simulations are performed and the contour of parasitic velocity magnitude and velocity vectors are shown for the two cases in Figs. 3.12 and 3.13, respectively. The main conclusions from these figures are listed as follows:

- The maximum parasitic current for case 2 is approximately 3 cm $\cdot$ s^{-1} whereas in case 3, this value does not exceed 20 μm $\cdot$ s^{-1}. The three orders of magnitude difference between the predicted velocities in the two cases, clearly shows the suppression of diffusion effects due to smaller time steps in case 3, in other words, smaller diffusion number.
- Although the contour of velocity in case 2 looks like a symmetric field around the centre of the bubble, velocity vectors in Fig. 3.12(b) exhibit a non-symmetric field outside of the bubble. This non-symmetric field is the cause of distortion of the bubble interface, regardless of accurate capturing of the interface thickness and pressure difference.
- Contrary to case 2, in case 3, the velocity field is perfectly symmetric, both inside and outside of the bubble. The vortices of parasitic currents are distributed symmetrically all over the interface of the bubble. This results in a minimised net translational motion of the bubble as well as the distortion of its interface.

Overall, it has been revealed that, to minimise the parasitic currents and capture the interface and pressure difference accurately, the Cn number should decrease and at the same time the time step should decrease in such a way to reduce the diffusion number as much as possible which means that the time step restriction by $maxCo$ is not sufficient and D is important as well, see section 2.4.2.

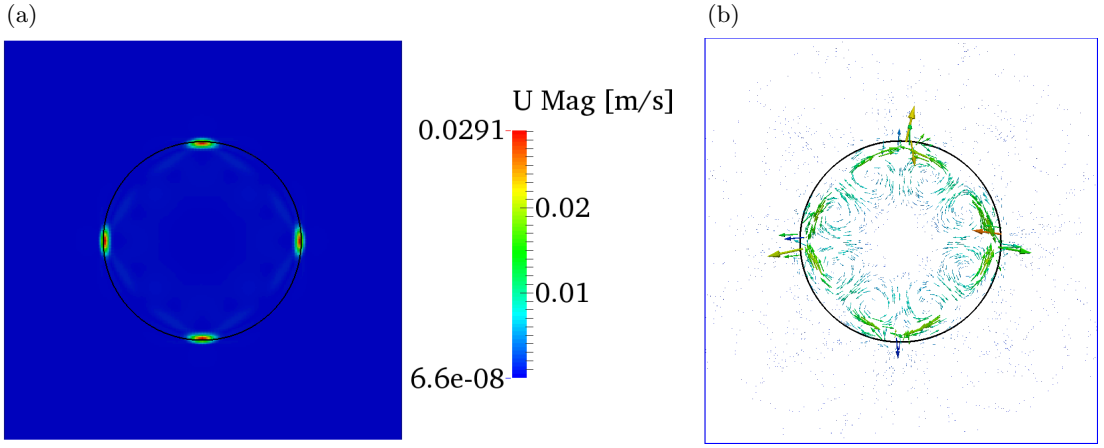

Figure 3.12.: Velocity field for the second case (a) and its vectors (b) using PFF with $D_B = 500$ μm, $N_C = 8$, $Cn = 0.016$, $\varepsilon = 8$ μm and $\kappa = 2.5 \times 10^{-12}m^3 \cdot$ s $\cdot$ kg^{-1}.

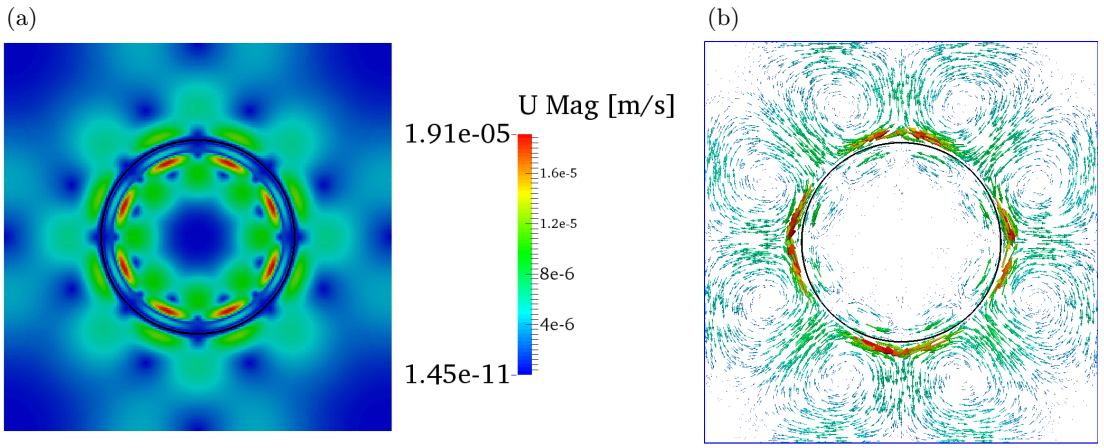

Figure 3.13.: Velocity field for the third case (a) and its vectors (b) using PFF with $D_B = 500\ \mu\text{m}$, $N_C = 8$, $Cn = 0.016$, $\varepsilon = 8\ \mu\text{m}$ and $\kappa = 2.5 \times 10^{-12}\text{m}^3 \cdot \text{s} \cdot \text{kg}^{-1}$.

It is reported in section 3.2.1 that the PFF solver does not conserve the mass as accurate as IF, since it always results in shrinkage of the bubble volume [18]. This shrinkage in the bubble volume owes its origin from the modelling of the phase field method. Therefore, it is suggested that to minimise this drawback, a plausible Cn number and a suitable mobility parameter κ should be chosen. In order to study the effect of mobility on the bubble shrinkage and consequently the mass conservation, the non-dimensional bubble diameter at different Cn numbers is plotted in Fig. 3.14, for cases with constant κ and variable κ as $G_\kappa \varepsilon^2$ with $G_\kappa = 0.1\ \text{m} \cdot \text{s} \cdot \text{kg}^{-1}$. It is depicted in this figure that, by increasing the Cn number, the bubble shrinks more and this effect is more significant for the case of variable κ. The maximum shrinkage occurs at $Cn = 0.04$, for which the assumption of variable κ leads to almost 2% reduction in the bubble terminal diameter. Therefore, in order to conserve mass, it is suggested that the value of Cn number should kept minimum. However, as it has been described before, lower Cn numbers require finer grids and hence, more computational time. Thus, a compromise is required in selecting the magnitude of Cn number.

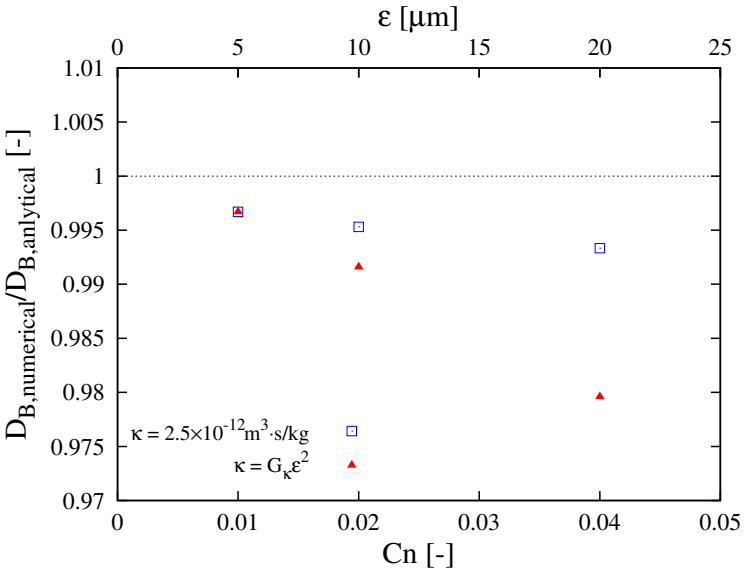

Figure 3.14.: Influence of the Cn number and κ on the non-dimensional terminal bubble diameter in PFF with $D_B = 500\ \mu\text{m}$, $N_C = 8$ and $G_\kappa = 0.1\ \text{m} \cdot \text{s} \cdot \text{kg}^{-1}$.

To quantify the shrinkage of the bubble surface, Fig. 3.15(a) and the accuracy of the PFF in conserving mass, the shift in the order parameter C vs. the Cn number should be

calculated. By definition, $-1 < C < 1$ and ideally, $\Delta C = 0$. However, using a theoretical method, Yue et al. [18] showed that the shift in C for a bubble in a 2D domain can be calculated as

$$\Delta C = -\frac{\sqrt{2}}{3} Cn. \tag{3.2}$$

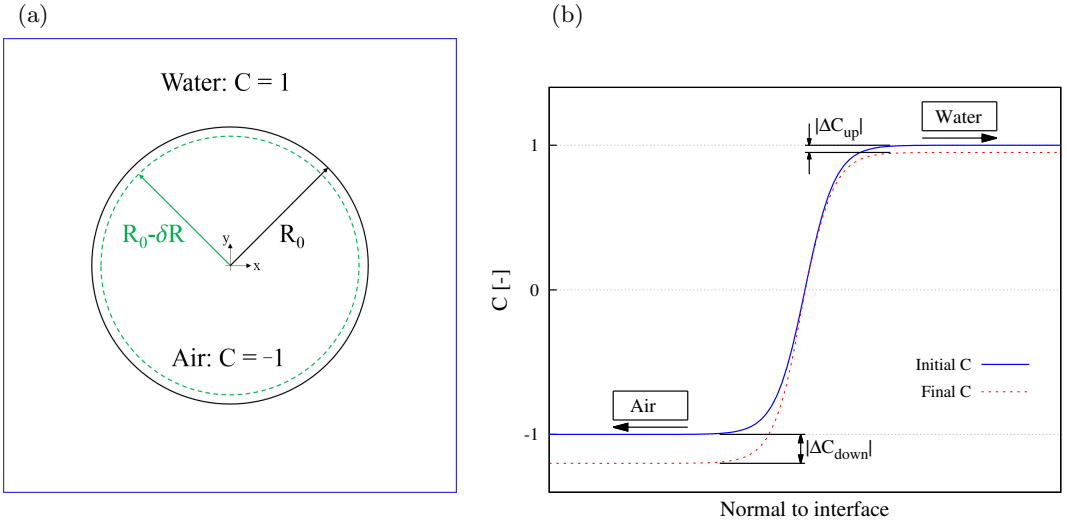

Figure 3.15.: Schematic illustration of (a) the shrinkage of an air bubble in water and (b) its order parameter distribution in the normal direction to interface.

This change results in an interval for C as $-1 - |\Delta C| < C < 1 - |\Delta C|$. The theoretical expected value for ΔC (i.e., zero), the theoretical approximation of it by Yue et al. [18] and its calculated value from the simulations are plotted in Fig. 3.16. The simulations give two different values, one for the air side and one for the water side of the interface, see Fig. 3.15(b). The average value of these two are plotted as well. It is worth-mentioning that the corresponding values for ΔC are different on water and air sides, which is not similar to the symmetric theoretical prediction in [18]. As illustrated, the average magnitude of ΔC and its ingredients on both sides are less than the theoretical approximation proposed by Yue et al. [18]. Hence, one can conclude that the PFF gives reasonable results in conserving the mass, especially at smaller Cn numbers. Moreover, the shrinkage of the bubble interface, obtained from simulations, in water side is negligible compared to its value in air side. The reasoning for the asymmetry of ΔC values on both sides and very small values of that in the water domain requires further research. Overall, one can conclude that, this curve is another evidence for deviation of PFF from mass conservation at higher Cn numbers. In addition, in selecting the suitable set of parameters for a simulation using PFF, the theoretical calculations could be used as a reasonable upper limit of the error in ΔC.

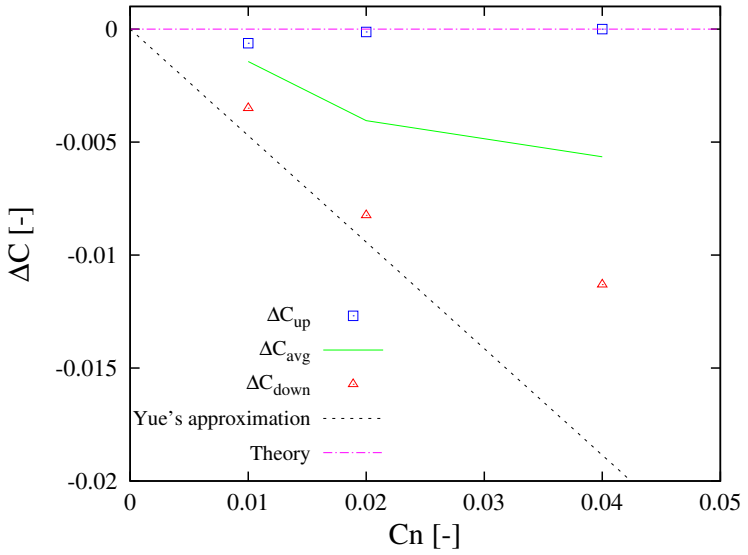

Figure 3.16.: Shrinkage of the bubble in PFF with $D_B = 500\ \mu\text{m}$, $N_C = 8$ and $\kappa = 2.5 \times 10^{-12}\text{m}^3 \cdot \text{s} \cdot \text{kg}^{-1}$

3.2.3. Influence of the Mobility

In order to investigate the sensitivity of the PFF solver to the mobility parameter κ, in this section, the results of two different cases with three orders of magnitude difference in κ are presented. These two values are $\kappa = 10^{-11}\text{m}^3 \cdot \text{s} \cdot \text{kg}^{-1}$ and $\kappa = 10^{-14}\text{m}^3 \cdot \text{s} \cdot \text{kg}^{-1}$. The maximum parasitic current and the non-dimensional displacement of centre of bubble are shown in Fig. 3.17. There is a difference between the terminal values of the two cases. Three orders of magnitude change in κ, leads to almost to two orders of magnitude variation in both $|\mathbf{U}_{max}|$ and x_D/D_B. Despite these changes, in both cases the maximum parasitic current does not create considerable velocity magnitudes and also does not lead the bubble to move significantly. It is depicted by these graphs that, increasing the mobility parameter affects the parasitic currents. However, as long as this parameter is within the range selected for this study, three orders of magnitude change in κ is not significant.

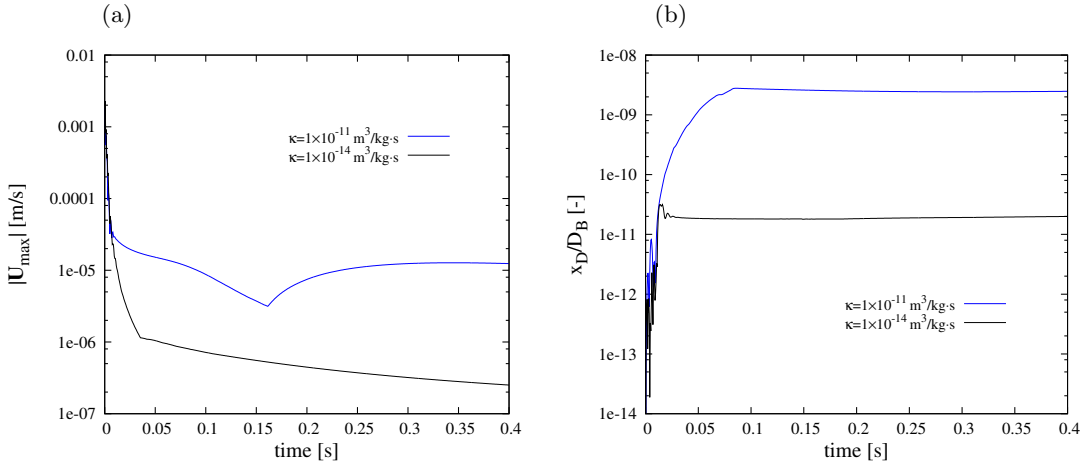

Figure 3.17.: Influence of κ on the time evolution of (a) the maximum parasitic current and (b) the non-dimensional displacement of centre of bubble in PFF with $D_B = 500\ \mu\text{m}$, $Cn = 0.02$, $N_C = 8$, $N_B = 100$ and $\varepsilon = 10\ \mu\text{m}$.

As a result, the change in mobility parameter does not affect the pressure difference prediction and the interface thickness too. This can be seen in Fig. 3.18. The diffusive

pattern of the solver is more evident in the pressure difference curve in Fig. 3.18(a) for $\kappa = 10^{-11}\mathrm{m}^3 \cdot \mathrm{s} \cdot \mathrm{kg}^{-1}$. However, no difference between the two cases can be distinguished in the order parameter curve in Fig. 3.18(b). These results also confirm that the most influencing parameter in minimising the parasitic currents and capturing the interface of the bubble is the Cn number.

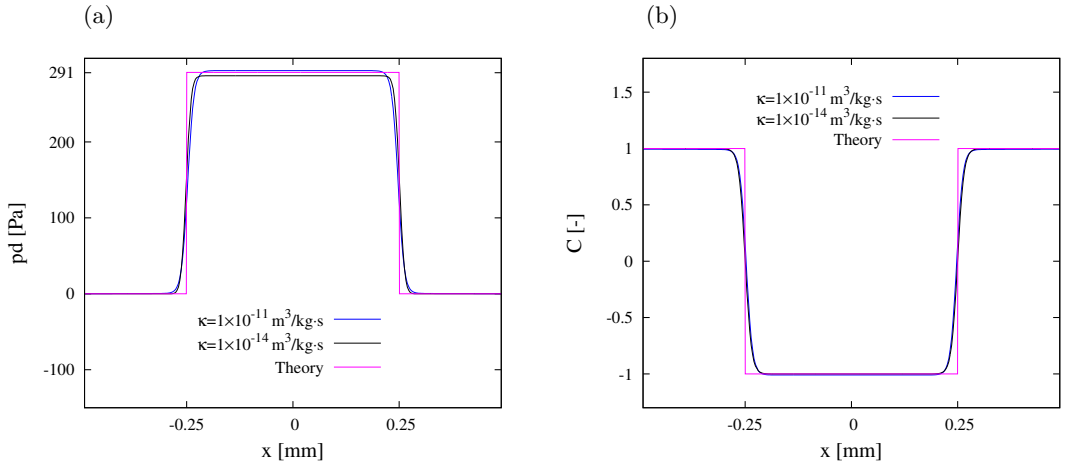

Figure 3.18.: Influence of κ on the (a) pressure and (b) phase distribution along the horizontal diameter of bubble in PFF with $D_B = 500$ μm, $Cn = 0.02$, $N_C = 8$, $N_B = 100$ and $\varepsilon = 10$ μm.

3.2.4. Variation of the Bubble Diameter

In this section, the results of the comparison between the two solvers for different bubble sizes are presented. It has been reported in the literature that the PFF solver, owing to its tendency to shrink the bubble size, does not work below a critical size and could even results in disappearance of the bubble [18]. To investigate the sensitivity of both IF and PFF to the initial bubble size, four different diameters, namely, 250 μm, 500 μm, 750 μm and 1 mm are selected and the fluid dynamics of them are studied, while the Eq. (3.1) is valid for all of the cases. The temporal resolution is defined by $maxCo = 0.1$ and $maxDeltaT = 5$ μs. The results of maximum parasitic current and bubble displacement are shown in Fig. 3.19, for fixed values of $Cn = 0.02$, $N_C = 8$ and $N_B = 100$. As expected, IF predicts a very large terminal parasitic velocity of about 1 $\mathrm{m} \cdot \mathrm{s}^{-1}$ for all of the bubble sizes. Since the mass of the gas inside the bubble increases by increasing the diameter, the inertia force required to move the bubble will be larger. Hence, the bigger the bubble at the same velocity, the smaller the movement of the centre of bubble, as it is depicted by Fig. 3.19(b). By contrast to IF, PFF predicts very small values for the maximum parasitic current and consequently the motion of the centre of bubble, except for the smallest bubble. Apparently, by decreasing the diameter to 250 μm, the maximum parasitic current reaches to ca. 0.1 $\mathrm{m} \cdot \mathrm{s}^{-1}$, which is relatively high compared to the ones for the other sizes. At the start of the simulation, the motion of the smallest bubble calculated by PFF is comparable with the results of IF. This is somehow in agreement with the theoretical prediction of the non-reliable results of PFF for smaller bubbles, as reported elsewhere [18]. More specifically, the critical bubble diameter, below which PFF finally results in disappearance of the bubble, reads

$$D_{B,crit} = \left(\frac{2\sqrt{6}}{\pi} V\varepsilon\right)^{1/3} \tag{3.3}$$

where V is the volume of the whole computational domain. For all the cases investigated here, one can see that $\varepsilon = 0.02 D_B$. In addition, $l_x = 2D_B$ and $l_y = 2D_B$ and hence, $V = 4{D_B}^2$. By substituting these values in Eq. 3.3, the critical diameter for all of the

cases can be approximated as $D_{B,crit} = 0.5D_B$. Thus, the smaller the bubble, the less is the distance between its actual and critical diameter and hence, the more the error in the PFF solver. This trend is observed in Fig. 3.19 as the numerical error increases when the bubble is smaller. Hence, one should pay attention in the accuracy of the solver, when small bubbles are of interest.

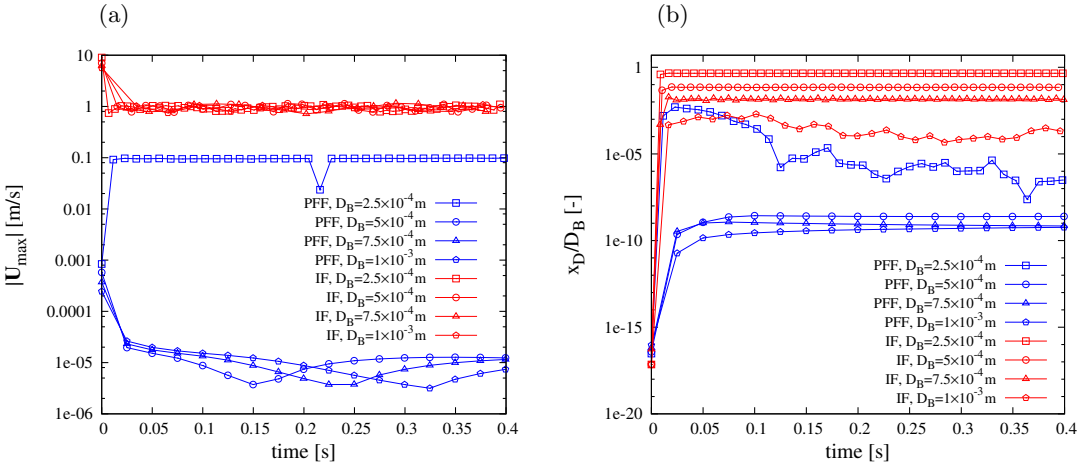

Figure 3.19.: Influence of the bubble size on the time evolution of (a) the maximum parasitic current and (b) the non-dimensional displacement of centre of bubble in IF and PFF with $Cn = 0.02$, $N_C = 8$ and $N_B = 100$.

Finally, the verification of the accuracy of the solvers is performed by the comparison between theoretical and numerical predictions of the pressure difference between inside and outside of the bubble. The results are shown in Fig. 3.20. The slope of these lines is supposed to be 2σ, according to the Young-Laplace equation. As it is illustrated in the figure, the PFF solver shows a very good agreement with theoretical values, especially for larger bubbles. For the bubble with $D_B = 250$ μm, there is a small difference between the results, whose reason is explained before. IF, however, shows a big discrepancy with theoretical prediction of the pressure difference for all bubble sizes. Moreover, the slope of the line, i.e., the value of surface tension, is predicted slightly different from the PFF. Overall, it is concluded that, for the bubbles which are not close to a critical size, the PFF solver is a good numerical tool to characterise their fluid dynamics in microfluidic devices.

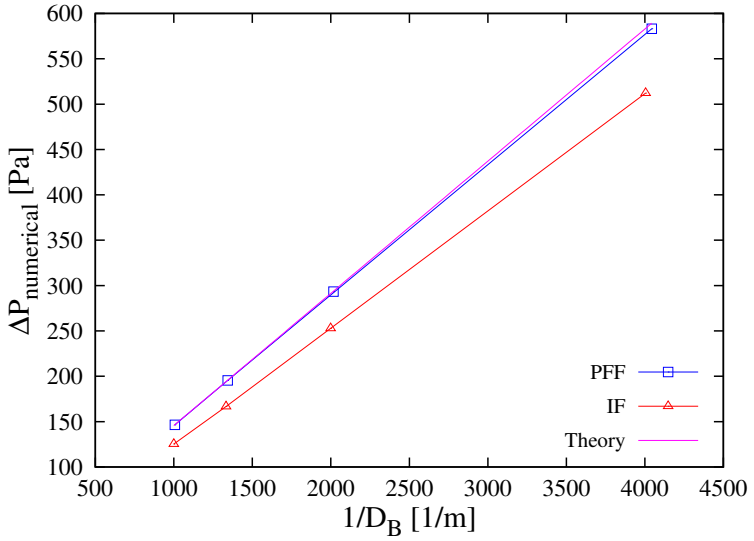

Figure 3.20.: Influence of bubble size on the terminal difference between the average pressures of air bubble and water in IF and PFF with $Cn = 0.02$, $N_C = 8$ and $N_B = 100$.

4. Conclusion

In this thesis, a thorough comparison between the Volume of Fluid (VOF) and Phase Field methods implemented in OpenFOAM package has been conducted to investigate the suitability of the methods for simulating multiphase flows. These methods are used in solvers *interFoam* (IF) and *phaseFieldFoam* (PFF), respectively. The case study is a 2D motionless air bubble in stagnant water. The comparison between the solvers is based on the sensitivity of the characteristic properties of a multiphase system and induced numerical parasitic current on the most important parameters affecting the fluid dynamics of such a system. The characteristic properties investigated are the bubble interface thickness and the pressure difference between the gas inside the bubble and the surrounding liquid. The parasitic current is characterised based on its maximum velocity, distortion of bubble shape and also motion of bubble centre induced by it. The investigated parameters include spatial and temporal resolutions of the numerical solvers, initial estimation for the bubble interface thickness and diffusivity (only applicable in PFF) and the bubble diameter.

The IF solver is not able to diminish the parasitic current sufficiently and cannot predict a symmetric velocity field inside and outside of the bubble. Therefore, the bubble distorts from its perfect circular shape assumed at the beginning of the simulation. Since these deviations are non-negligible in some cases, the physical characteristic properties, such as the pressure difference between inside and outside of the bubble are predicted with large errors. These discrepancies cannot be removed by mesh refinement; although better accuracy is seen in prediction of the interface thickness and diameter of the bubble as the grid becomes finer. This indicates that the solver conserves the mass of both phases accurately and the numerical diffusion of the VOF method could be mitigated by increasing the mesh resolution; which in turn increases required computational costs.

The PFF solver, on the other hand, estimates the maximum parasitic current and the displacement of bubble centre, orders of magnitude smaller than the values obtained by IF. Thus, PFF is considered to be more accurate in predicting the equilibrium state of the bubble with negligible parasitic currents. Nonetheless, one should pay attention in selecting the spatial resolution of the grid required to estimate the interface at the start of the simulation. It is shown that at least six cells for the resolution of diffuse interface are needed to have an accurate prediction of the bubble state, and by doing so, the solver performs quite well, almost regardless of the grid resolution outside of the interface region. This good performance is observed in estimating the pressure difference between inside and outside of the bubble, bubble habitat due to negligible parasitic velocity and bubble

shape due to symmetry of the parasitic current. Therefore, it is concluded that the solver is capable of capturing the essential physics involved.

The main disadvantage of PFF, however, appears in mass conservation for the gas phase inside the bubble, since the solver has the intention to shrink the bubble. This problems becomes more significant when the Cn number (a measure of the interface thickness) increases. The problem is presumably due to numerical diffusive properties of the solver, also observed in predicting the interface thickness. The other origin of this deviation is inherited in the definition of the perfect interface as $C = 0$ inside the interval $-1 < C < 1$. The appeared shift in the interval, i.e., ΔC results in another position for isoline $C = 0$, which at the end of simulation is not in the same place as before and therefore, an error appears in the final size of the bubble. In this study, the shrinkage of the bubble is calculated smaller than its expected value from theoretical predictions. Moreover, from theory, the shrinkage of the bubble is supposed to be symmetric in both gas and liquid sides; whereas in this study, it is calculated much less in the water side. The reason for this asymmetry is unknown and requires further studies. Due to the diffusive nature of the solver, this issue becomes more notable for smaller bubbles and there exists a critical size for the bubble diameter, below which the solver tends to disappear the bubble completely. It is shown that for the considered cases in this thesis, the smaller the bubble, the closer the actual and critical bubble sizes. Therefore, attention should be paid in the accuracy of PFF, when small bubbles (which are typically present in microfluidic systems) are of interest.

To overcome the issue regarding this shrinkage and consequently to conserve mass, refining the mesh close to the bubble interface is suggested in this study. The latter is possible to do by keeping the Cn number as small as possible. However, lower Cn numbers require finer grids and hence, more computational time. Thus, one should compromise between accuracy and hence consistency of PFF by selecting a smaller Cn number and required computational resources. Obviously, the resources for 3D cases would be significantly more. Nonetheless, the adopted 2D approach in this study is undoubtedly beneficial for appointing an effective numerical tool to design and optimise microfluidic systems involving multiphase flows.

Symbols and Abbreviations

Latin Symbols

Symbol	Unit	Description
C	[−]	Order parameter for phase identification
Ca	[−]	Capillary number
Cn	[−]	Cahn number
Co	[−]	Courant number
D	[−]	Diffusion number
D_B	[m]	Bubble Diameter
D_D	[m]	Droplet Diameter
$\mathcal{F}$	$[\mathrm{N} \cdot \mathrm{m}]$	Mixing energy functional
$\mathbf{F}_\sigma$	[N]	Surface tension force
g	$[\mathrm{m} \cdot \mathrm{s}^{-2}]$	Acceleration of gravity
G_κ	$[\mathrm{m} \cdot \mathrm{s} \cdot \mathrm{kg}^{-1}]$	Pre-factor in the relation between the mobility and capillary width square
l	[m]	Length
l_C	[m]	Interface thickness
$\mathbf{n}$	[−]	Normal vector
N	[−]	Number of cells
N_B	[−]	Number of cells for bubble
N_C	[−]	Number of cells for interface
N_D	[−]	Number of cells for droplet
Oh	[−]	Ohnesorge Number
p	[Pa]	Pressure
p_{avg}	[Pa]	Average pressure
STD_{D_B}	[m]	Standard deviation of bubble diameter
$\mathbf{U}$	$[\mathrm{m} \cdot \mathrm{s}^{-1}]$	Velocity
$\lvert\mathbf{U}_{max}\rvert$	$[\mathrm{m} \cdot \mathrm{s}^{-1}]$	Maximum parasitic current
(x, y, z)	$[(\mathrm{m}, \mathrm{m}, \mathrm{m})]$	Spatial Cartesian coordinates
x_D	[m]	displacement of centre of bubble

Greek Symbols

Symbol	Unit	Description
α	[−]	Phase fraction
Γ	$[\mathrm{m}^2 \cdot \mathrm{s}^{-1}]$	Diffusion coefficient
δ	$[\mathrm{m}^{-1}]$	Delta function
Δ	[−]	Difference

ε	[m]	Capillary width
$\mathcal{K}$	$[\mathrm{m}^{-1}]$	Curvature
κ	$[\mathrm{m}^3 \cdot \mathrm{s} \cdot \mathrm{kg}^{-1}]$	Mobility
λ	[N]	Mixing energy density
μ	$[\mathrm{Pa} \cdot \mathrm{s}]$	Dynamic viscosity
ν	$[\mathrm{m}^2 \cdot \mathrm{s}^{-1}]$	Kinematic viscosity
ρ	$[\mathrm{kg} \cdot \mathrm{m}^{-3}]$	Density
σ	$[\mathrm{kg} \cdot \mathrm{s}^{-2}]$	Interfacial tension coefficient
ϕ	$[\mathrm{N} \cdot \mathrm{m}^{-2}]$	Chemical potential

Subscripts

Symbol	Description
a	Air
C	Centre of bubble
D	Displacement
g	Gas
i	Initial condition
l	Liquid
w	Water

Abbreviations

Abbreviation	Description
1D	One Dimensional
2D	Two Dimensional
3D	Three Dimensional
CAE	Computer Aided Engineering
CFD	Computational Fluid Dynamics
CSF	Continuum Surface Force
IF	interFoam
ISTM	German: Institut für Strömungsmechanik
KIT	Karlsruhe Institute of Technology
l.h.s	Left-Hand Side
NSE	Navier-Stokes Equations
PFF	phaseFieldFoam
r.h.s	Right-Hand Side
STD	Standard Deviation
VOF	Volume of Fluid

List of Figures

List of Tables

Bibliography

[1] G.M. Whitesides. The origins and the future of microfluidics. *Nature Publishing Group*, 442(7101):368–73, 2006.

[2] OpenFOAM, The OpenFOAM Foundation. `http://www.openfoam.org`.

[3] F.M. White. *Fluid Mechanics, 4^{th} Edition.* McGraw-Hill Higher Education, 1998.

[4] B. Lautrup. *Physics of Continuous Matter: Exotic and Everyday Phenomena in the Macroscopic World, 2^{nd} Edition.* CRC Press, 2011.

[5] H. Marschall, X. Cai, M. Wörner, O. Deutschmann. Development of Phase Field methods using OpenFOAM – part I: Method development and implementation. 2016. 10th International OpenFOAM Workshop, Ann Arbor, Michigan, USA, June 29 – July 2.

[6] D. Jacqmin. Calculation of two-phase Navier-Stokes flows using phase-field modeling. *Journal of Computational Physics*, 155(1):96 – 127, 1999.

[7] B. Lafaurie, C. Nardone, R. Scardovelli, Stéphane Zaleski, G. Zanetti. Modelling merging and fragmentation in multiphase flows with surfer. *Journal of Computational Physics*, 113(1):134 – 147, 1994.

[8] M.M. Francois, S.J. Cummins, E.D. Dendy, D.B. Kothe, J.M. Sicilian, M.W. Williams. A balanced-force algorithm for continuous and sharp interfacial surface tension models within a volume tracking framework. *Journal of Computational Physics*, 213(1):141 – 173, 2006.

[9] J.U. Brackbill, D.B Kothe, C. Zemach. A continuum method for modeling surface tension. *Journal of Computational Physics*, 100(2):335 – 354, 1992.

[10] D.J.E. Harvie, M.R. Davidson, M. Rudman. An analysis of parasitic current generation in Volume of Fluid simulations. *Applied Mathematical Modelling*, 30(10):1056 – 1066, 2006.

[11] K. Yokoi. A density-scaled continuum surface force model within a balanced force formulation. *Journal of Computational Physics*, 278:221 – 228, 2014.

[12] S.S. Deshpande, L. Anumolu, M.F. Trujillo. Evaluating the performance of the two-phase flow solver interfoam. *Computational Science & Discovery*, 5(1):014016, 2012.

[13] A. Albadawi, D.B. Donoghue, A.J. Robinson, D.B. Murray, Y.M.C. Delauré. Influence of surface tension implementation in Volume of Fluid and coupled Volume of Fluid with Level Set methods for bubble growth and detachment. *International Journal of Multiphase Flow*, 53:11 – 28, 2013.

[14] V. Dyadechko, M. Shashkov. Reconstruction of multi-material interfaces from moment data. *Journal of Computational Physics*, 227(11):5361 – 5384, 2008.

[15] R. Acar. Simulation of interface dynamics: a diffuse-interface model. *The Visual Computer*, 25(2):101–115, 2009.

[16] H.G. Lee, J. Kim. Regularized Dirac delta functions for Phase Field models. *International Journal for Numerical Methods in Engineering*, 91(3):269–288, 2012.

[17] Q. He, N. Kasagi. Phase-Field simulation of small capillary-number two-phase flow in a microtube. *Fluid Dynamics Research*, 40(7-8):497, 2008.

[18] P. Yue, C. Zhou, J.J. Feng. Spontaneous shrinkage of drops and mass conservation in phase-field simulations. *Journal of Computational Physics*, 223:1–9, 2007.

[19] M. Wörner. *A Compact Introduction to the Numerical Modeling of Multiphase Flows.* Forschungszentrum Karlsruhe Technik und Umwelt. Forschungszentrum Karlsruhe, 2003.

[20] C.W. Hirt, B.D. Nichols. Volume of Fluid (VOF) method for the dynamics of free boundaries. *Journal of Computational Physics*, 39(1):201 – 225, 1981.

[21] Y. Renardy, M. Renardy. PROST: A parabolic reconstruction of surface tension for the Volume-of-Fluid method. *Journal of Computational Physics*, 183(2):400 – 421, 2002.

[22] X. Cai, M. Wörner, O. Deutschmann. Implementation of a Phase Field method in OpenFOAM for simulation of spreading droplets and verification by test problems. 2013. In Proceedings of 7th Open Source CFD International Conference, Hamburg, Germany, October 24-25,.

[23] X. Cai, M. Wörner, H. Marschall, O. Deutschmann. Numerical study on the wettability dependent interaction of a rising bubble with a periodic open cellular structure. *Catalysis Today*, 273:151 – 160, 2016. 5th International Conference on Structured Catalysts and Reactors, ICOSCAR-5, Donostia-San Sebastián, Spain, 22-24 June,.

[24] J. Fröhlich. *Large Eddy Simulation turbulenter Strömungen.* Lehrbuch : Maschinenbau. Teubner Verlag, 2007.

[25] ParaView. `http://www.paraview.org`.

[26] S. Popinet, S. Zaleski. A front-tracking algorithm for accurate representation of surface tension. *International Journal for Numerical Methods in Fluids*, 30:775–793, July 1999.

[27] M. Bussmann, S. Chandra, J. Mostaghimi. Modeling the splash of a droplet impacting a solid surface. *Physics of Fluids*, 12(12):3121–3132, 2000.

[28] S.S. Deshpande, M.F. Trujillo, X. Wu, G. Chahine. Computational and experimental characterization of a liquid jet plunging into a quiescent pool at shallow inclination. *International Journal of Heat and Fluid Flow*, 34:1 – 14, 2012.

[29] E. Berberovic, N.P. van Hinsberg, S. Jakirlić, I.V. Roisman, Cameron Tropea. Drop impact onto a liquid layer of finite thickness: Dynamics of the cavity evolution. *Physical Review E*, 79(3), 2009.

[30] M.F. Trujillo, J. Alvarado, E. Gehring, G.S. Soriano. Numerical simulations and experimental characterization of heat transfer from a periodic impingement of droplets. *ASME. J. Heat Transfer*, 133:122201–122201–10, 2011.

[31] CFD Online, Online center for Computational Fluid Dynamics. `http://www.cfd-online.com`.

Appendix

A. OpenFOAM Codes

The codes are based on codes in [31].

A.1. Initial Definition of a Bubble in interFoam

system/setFieldsDict

```
defaultFieldValues   (volScalarFieldValue      alpha1      1);
regions              (cylinderToCell {
                                     p1          (0 0 -0.5e-6);
                                     p2          (0 0 0.5e-6);
                                     radius      250e-6;
                                     fieldValues (volScalarFieldValue    alpha1    0);
                                     }
                     );
```

Note: In the code, radius should be given which is half of the diameter. $p1$ and $p2$ are the two ends of cylinder centre line.

A.2. Initial Definition of a Bubble in phaseFieldFoam

```
radius=250e-6
cx=0.0 The initial x coordinate of centre of bubble
cy=0.0 The initial y coordinate of centre of bubble
epsilon=1e-5 The interface width is the same as epsilon in constant/phaseFieldProperties
funkySetFields -time 0 -field C -keepPatches
-expression "tanh((sqrt(sqr(pos().x-$cx)+sqr(pos().y-$cy))-$radius )/(sqrt(2)*$epsilon))"
```

A.3. Maximum Parasitic Current

```
In system/controlDict as a function
velocityExtreme {
  type                swakExpression;
  outputControlMode   timeStep;
  outputInterval      1;
  ValueType           internalField;
  verbose             true
  expression          "mag(U)";
  accumulations       (max);
                }
```

A.4. Position of the Centre of Bubble

```
In system/controlDict as a function
xCentreOfBubble {
  type                swakExpression;
  outputControlMode   timeStep;
  outputInterval      1;
  ValueType           internalField;
  verbose             true
  expression          "(1-alpha1)*vol()*pos().x/sum((1-alpha1)*vol())"; //interFoam
  expression          "(1-C)*vol()*pos().x/sum((1-C)*vol())"; //phaseFieldFoam
  accumulations       (sum);
                    }
```

Note: In y direction analogue to x direction.

A.5. Definition of the Interface

```
In system/controlDict as a function
interfaceMiddle {
  type              surfaces;
  outputControl     outputTime;
  surfaceFormat     raw;
  fields            ();
  surfaces          (interfaceMiddle {
                                        type          isoSurface;
                                        isoField      alpha1; //interFoam
                                        isoValue      0.5; //interFoam
                                        isoField      C; //phaseFieldFoam
                                        isoValue      0; //phaseFieldFoam
                                        interpolate   true;
                                        }
                    );
                    }
```

Note: Analogue for interfaceNearToWater ($alpah1 = 0.9$ and $C = 0.9$) and for interfaceNearToBubble ($alpah1 = 0.1$ and $C = -0.9$).

A.6. Average Pressure Difference

```
In system/controlDict as a function
pAverageWater {
  type                swakExpression;
  outputControlMode   outputTime;
  ValueType           internalField;
  verbose             true
  variables           (
                      "thresW=0.99;"  //interFoam
                      "volWater=(alpha1>thresW?vol():0);" //interFoam
                      "volWater=("pWater=(alpha1>thresW?p:0);" //interFoam
                      "thresW=0.98;"  //phaseFieldFoam
                      "volWater=(C>thresW?vol():0);" //phaseFieldFoam
                      "volWater=("pWater=(C>thresW?p:0);" //phaseFieldFoam
                      );
  expression          "pWater*volWater/sum(volWater)";
  accumulations       (sum);
                }
```

```
In system/controlDict as a function
pAveragBubble {
  type                swakExpression;
  outputControlMode   outputTime;
  ValueType           internalField;
  verbose             true
  variables           (
                      "thresB=0.01;"  //interFoam
                      "volBubble=(alpha1<thresB?vol():0);" //interFoam
                      "volBubble=("pBubble=(alpha1<thresB?p:0);" //interFoam
                      "thresB=-0.98;"  //phaseFieldFoam
                      "volBubble=(C<thresB?vol():0);" //phaseFieldFoam
                      "volBubble=("pBubble=(C<thresB?p:0);" //phaseFieldFoam
                      );
  expression          "pBubble*volBubble/sum(volBubble)";
  accumulations       (sum);
                }
```